Two-dimensional Metal-Organic Framework (MOF) and Covalent-Organic Framework (COF): Synthesis and their Energy-related Applications

Weiran Zheng,† Chui-Shan Tsang,† Lawrence Yoon Suk Lee,* and Kwok-Yin Wong*

Department of Applied Biology and Chemical Technology and the State Key Laboratory of Chemical Biology and Drug Discovery, The Hong Kong Polytechnic University, Hung Hom, Kowloon, Hong Kong SAR

** Corresponding authors: lawrence.ys.lee@polyu.edu.hk, kwok-yin.wong@polyu.edu.hk*

† These authors contributed equally to this work.

1. Introduction

The development of two-dimensional (2D) materials with nanosize thickness is getting more and more attention due to its unique and tunable properties that are useful in a wide range of applications, especially in energy conversion and storage.[1-3] Comparing with 3D materials, 2D materials have been considered as a better candidate for catalysis, as they exhibits larger specific surface areas and higher surface-to-volume ratios, which can provide more active sites available for target substrates. In addition, the transport of charge carriers and photons is strictly confined in the 2D space, which would make remarkable differences in the electronic and optical properties. For these expected advantages, various 2D materials, such as MXenes[4-6], graphitic carbon nitride,[7-9] and layered double hydroxides,[10-12] have been extensively explored in the research fields of energy conversion and storage recent years.[3] Among them, 2D materials with porous structure are of particular interests since their interaction with substrate ions or molecules is not limited only on their surface, but the entire materials including the core area can be also utilized.[13-15] The performance of porous materials highly depends on its structure, wherein crystalline network is always more preferable than the amorphous one. Hence, it is of crucial importance to carefully control the uniformity and distribution of pore size, shape, and atomic composition, and volumes of the void spaces in order to obtain a desired structure with well-defined pores with monodisperse size distribution, stability, and tunable metrics.[16]

Metal-organic frameworks (MOFs) and covalent-organic frameworks (COFs) are crystalline porous materials that best suit for all the requirements that previously mentioned. In both systems, the structure and functionality of pores can be tailor-made for a specific function using various chemical and physical approaches. Building blocks of different structure and chemical properties can be rationally and systematically combined and synergistically function within the framework.

Moreover, their ultrahigh porosity structures lead to high surface-to-volume ratio, even in 3D structures, facilitating the easy access of ions or molecules towards the active sites in the frameworks. MOFs and COFs, therefore, have received great attention from the researchers in energy conversion and storage fields.[17-20] Recently, the number of reports on fabricating MOFs and COFs in 2D structures has rapidly increased, most of which target to maximize the advantages of porous materials by increasing the exposed surface area.

In this review, we aim to provide an overview on the synthesis of 2D MOFs and COFs based on self-assembly and other newly developed methods. The application of both 2D MOFs and COFs in energy conversion reactions and storage will also be summarized with outlooks on research direction.

2. Synthesis

2.1. 2D metal-organic frameworks (2D-MOFs)

MOFs are a subclass of coordination polymers with permanent porosity usually in a three dimensional network structure. It is constructed by the coordination between metal nodes (metal ions or metal clusters) and organic linkers (polytopic ligands) which results in the formation of an open framework structure in different dimensionalities. Different from 3D MOFs, 2D MOFs are built by the stacking of single MOF layers *via* weak intermolecular forces. The coordination geometry of metal nodes and organic ligands play the paramount role in guiding the formation of the single layer with metal–ligand bond spread over the polymer in one direction. In the formation of 2D MOFs, the structure of ligand determines the size and functionality of the resulting pores in the framework. Besides, it also controls the superimposition of the layers, either in eclipsed or staggered mode, through weak interactions including π-π stacking, van der Waals force, and

hydrogen bonding. In the following section, we will discuss various synthetic approaches developed for constructing 2D MOFs.

2.1.1. Self-assembly approaches

2D MOFs can be fabricated by the self-assembly process where the specific coordination between the metal nodes and organic ligands determine the morphology without any external forces or supports engaged. According to the geometrical information that are carried by metal nodes and organic ligands, 2D MOFs with different morphologies as well as pore sizes and structures can be afforded.

(a) Self-assembly with single-type of ligand

2D MOF can be constructed by a single-type of ligand that has two or more binding groups of appropriate coordination angle. A full list of such ligands reported so far is given in **Figure 1**. The simplest type of ligands used in 2D MOFs is flexible aliphatic organic ligands, such as hydroxyacetic acid (**1**),[21] 2,2′-[(2-methyl-2-nitropropane-1,3-diyl)diamino]diacetate (**2**),[22] and adipic acid (hexandioic acid, **3**).[23] Sudarsankumar *et al*. reported 2D Ce–adipate MOF that was prepared by the reaction of with $Ce(NO_3)_3$ and adipic acid.[23] Each adipate ligand adopts a tridentate chelating bridging mode μ^2-η^2:η^1 to coordinate with two Ce^{3+} ions, which leads to the formation of 2D framework with the single layer comprised with infinite chains of edge sharing $CeO_6(H_2O)_2(NO_3)$ polyhedron. The stacking between single layers results in the formation of an elongated hexagonal bullet-shaped channels along *c*-axis.

In general, aromatic ligands are more preferable for the construction of 2D MOFs than aliphatic ones. The rigid structure of aromatic rings make the design and prediction of 2D MOF structure is easier, and various ligands with an aromatic ring in the center were reported (**4**-**9**).[23-29] Especially, polyprotic aromatic ligands with carboxylate groups at 1 and 4 positions, such as 1,4-

benzenedicarboxylic acid (H_2bdc, **7**) and 2,2′-dithiodibenzonic (DTBA, **9**), are popularly used. The H_2bdc has been coordinated to the first-row transition metal ions to yield various 2D MOFs.[27, 28] For example, Bagherzadeh *et al*. reported a 2D Co-MOF,[27] where metal clusters made of metal ions and oxygen atoms were used as metal node. These metal clusters are often called as a secondary building unit (SBU) and provide simpler coordination angle than metal ions at the metal node positions. The coordination of bdc^{2-} ligand with two Co SBU units in either bidentate bridging μ_2-η^1:η^1 or tridentate chelating bridging μ_2-η^2:η^1 mode resulted in the 2D structure of Co MOF. The aromatic ligands containing N, such as pyridine, are often used in 2D MOFs (**10**-**12**).[30-33] Michaelides *et al*. reported a 2D La(III) MOF which is afforded by the reaction of La^{3+} and 4-hydroxypyridine-2,6-dicarboxylic acid (H_3chel, **8**) at pH 5.4.[23] Two O atoms of two carboxylate groups and one N atom of pyridine are coordinated with one La^{3+} ion, while the other two O atom of the carboxylate groups are coordinated to another two La^{3+} ions. Each $(Hchel)^{2-}$ ligand is either coordinated to one or two La^{3+} ions in a chelating bridging mode. Such coordination results in the formation of a single layer parallel to the (001) plane, and van der Waals interaction, π-π stacking, and hydrogen bonding among the layers yield a 2D framework. Reaction of 2,2′-bipyridine-5,5′-dicarboxylic acid (BDA, **11**) with first-row transition metals (M^{2+}= Zn^{2+}, Co^{2+} and Ni^{2+}) was also reported to afford by Park *et al*.[32] The BDA ligand is coordinated with three M^{2+} ions: one of them is coordinated with the bidentate bipyridine, and the others are coordinated with the O atoms from the carboxylates groups in either monodentate or bidentate bridging μ_2-η^1:η^1 mode. The single layers resulted from these coordinations are stacked together *via* π-π stacking interaction to result in a 2D network.

An interesting 2D Zn MOF with pores in hexagonal shape is reported by Tang *et al*. using 4, 4′-(2,2-diphenylethene-1,1-diyl)dibenzoic acid (DEDB, **13**).[34] Each carboxylate group of the

ligand is coordinated with two Zn^{2+} ion of a Zn_4O tetranuclear octahedron SBU in bidentate bridging μ_2-η^1:η^1 mode, leading to the formation of Kagome-type 2D single layer. Two benzene rings without any functional groups contribute to the stabilization of stacking layers by providing C–H···π interactions, forming the overall framework with hexagonal pores.

Ligands with higher symmetry, such as C_3, C_4, and D_{4h} symmetry, have been considered for the formation of 2D MOF. Ligands with C_3-symmetry include 1,3,5-benzenetricarboxylic acid (H_3BTC, **14**), 3,3′,3″-(benzene-1,3,5-triyl)tris(pentane-2,4-dione) (BTPD, **15**), and tris(4′-carboxylbiphenyl)-amine (TCBPA, **16**).[35-37] Liu *et al*. reported the formation of an interesting Chinese pane-like 2D Ln MOF, $[Dy(TCBPA)(H_2O)_2]_n$ using TCBPA.[37] In the framework structure, $TCBPA^{3-}$ exhibits two different coordination modes. Two carboxylate groups are coordinated with two discrete Dy^{3+} ions in bidentate chelating mode, while the remaining one is coordinated with another two discrete Dy^{3+} ions in bidentate bridging μ_2-η^1:η^1 mode.

Tetrakis(4-pyridyl)-1,2,9,10-diethano[2.2]paracyclophane (TPDP, **17**) and 1,1,2,2-Tetra(4-(4-carboxylphenyl)benzyl)ethene (TCBPE, **18**) possess C_4 and D_2 symmetry, respectively. TPDP was reported to coordinate with four discrete Co^{2+} ions with N atoms from pyridine rings, which results in a 2D framework of alternating rows of square and hexagon cavities.[38] Wang *et al*.[39] showed that TCBPE react with Co^{2+} ions to afford a 2D MOF, where each carboxylate group of the ligand is coordinated two Co^{2+} ions from paddle-wheel $Co_2(COO)_4$ clusters in bidentate bridging μ_2-η^1:η^1 mode to afford a 2D single layer. Stabilized by π-π stacking interaction, the layers are stacked together in a staggered configuration.

For designing 2D MOF structures with good electron conductivity, highly conjugated ligands with D_{3h} symmetry are attractive, which include benzenehexathiol (BHT, **19**), triphenylene-2,3,6,7,10,11-hexathiolate (THT, **20**), and 2,3,6,7,10,11-hexaaminotriphenylene (HATP, **21**).[40-

44] For example, the liquid–liquid interfacial synthetic method was developed by Nishihara *et al*. for the preparation of 2D Ni MOFs. At the liquid interface, BHT in the organic layer was overlaid on $Ni(OAc)_2$ in aqueous layer through the coordination between the S of BHT and Ni^{2+} ions. A single layer produced in such a way further stack together in staggered configuration *via* π-π stacking interactions afford a 2D network. (Figure 20)

Ligands bearing the porphyrin moiety with D_{4h} symmetry (**22**-**24**) are one of the most popular choices in the formation of 2D MOFs. Vittal *et al*. reported a 2D MOF self-assembled from 5, 10, 15, 20-tetra-4-pyridyl-21H, 23H-porphine (TPyP, **23**) and $Cu_2(OAc)_4$.[45] TPyp coordinates with four discrete Cu^{2+} ions *via* N atoms of four pyridine moieties to give an undistorted square grid single layer for the framework. Each layer stacks with each other in staggered configuration to form a 2D network without interpenetration. With tetra(4-carboxylphenyl)porphyrin (TCPP, **24**), monometallic and bimetallic 2D MOFs have been reported through the coordination between carboxylate groups and discrete metal ions. [46-48] Phthalocyanine-based ligand is recently gaining popularity due to its interesting electrical properties.[49, 50] For example, Du *et al*. reported the complexation of 2,3,9,10,16,17,23,24-octa-amino-phthalocyaninato (OAPc, **22**) with Ni^{2+} ions that affords 2D Ni MOF.[50]. (Figure 18)

(b) Self-assembly with two types of ligands

Limited by the number of possible coordination angles, it could be challenging to precisely control the formation of 2D MOF with single type of ligand. Moreover, available ligands that can form 2D structure are limited because of the difficulty in ligand synthesis, which reducing the tunability of 2D MOF properties for various applications. These shortcomings can be solved by using more than one type of ligands. **Table 1** shows the combination of ligands and metal nodes that have been used for the construction of hetereogenous 2D MOFs. Feng and co-workers reported

two 2D Cu MOFs based on 1,2,4-benzenetricarboxylate (1,2,4-BTC) and 4,4′-bipyridine (bpy), $[Cu_3(1,2,4\text{-}BTC)_2(bpy)(H_2O)_4]$ and [Cu(1,2,4-HBTC)(bpy)], which were synthesized in water and a mixture of water and 1-butanol, respectively.[51] The single layer of $[Cu_3(1,2,4\text{-}BTC)_2(bpy)(H_2O)_4]$ is composed of two different 1D chains, $[Cu_2(1,2,4\text{-}BTC)2]_n^{2n-}$ and $Cu(bpy)]_n^{2n+}$, wherein N atoms of bpy are coordinated with two discrete Cu^{2+} ions in $Cu(bpy)]_n^{2n+}$. In $[Cu_2(1,2,4\text{-}BTC)_2]_n^{2n-}$, the carboxylate groups on 1- and 4-positions of the BTC ligand are coordinated with two discrete Cu^{2+} ions in monodentate mode, while the other carboxylate group on 2-position is coordinated with the Cu^{2+} ion bonded to bpy. As a result, single layer with an interesting step-like structure has been resulted and the stacking of these layers through hydrogen bonding between coordinated water molecule and carboxylate group of the ligand yields a 2D network. On the other hand, 1,2,4-BTC ligand in [Cu(1,2,4-HBTC)(bpy)] is coordinated with two discrete Cu^{2+} ions from paddle wheel cluster $Cu_2(COO)_4(bpy)_2$ to result in a single layer of the framework. These layers are stacked together to afford 2D network *via* π-π interaction.

Another example worth to mention is 2D Co MOF prepared with 2,3,6,7,10,11-hexaaminotriphenylene (HATP) and triphenylene-2,3,6,7,10,11-hexathiolate (THT).[52] Using Langmuir–Blodgett technique, Dong *et al*. synthesized single-layer 2D Co MOF, in which the CoS_2N_2 complexes along with the CoN_4 and CoS_4 moieties were incorporated into the hexagonal networks through metal dithiolene-diamine coordination. As a consequence, those highly active catalytic centers embedded in 2D Co MOFs allowed its application for electrocatalysis of hydrogen evolution reaction.

Table 1. Combination of ligands and metal nodes in the construction of hetereogenous 2D MOF

Ligands	Metal node	Reference
	$Cu_2(COO)_4$ paddlewheel cluster or Cu^{2+} ion	[51]

$Cu_2(COO)_4$ paddlewheel cluster	[53, 54]
Cu^{2+} ion	[55]
Co^{2+} ion	[52]
Cu^{2+} ion	[56]
Zn^{2+} or Cu^{2+} ion	[57]
$Zn_2(COO)_4$ paddlewheel cluster	[58]

2.1.2. Template-directed synthesis

Although the template-directed synthesis is widely adopted in many other fields, synthesis of 2D MOFs using a template is rarely reported, except for one case with ZIF-67. ZIF-67, one of the most studied MOFs, has a well-defined 3D structure. By using a salt template method to confine the growth of the framework, Dong *et al*. prepared a 2D ZIF-67.[59] They mixed a methanolic solution of $CoCl_2$ and 2-methylimidazole with a large quantity of NaCl powder under vigorous stirring resulted in the formation of ZIF-67 nanosheet. Limited by the volume of solvent used and therefor limited amount of precursors, the growth space and direction of ZIF-67 are confined and only grow along the microcrystal plane of salt. As a result, an ultrathin 2D ZIF-67 nanosheet was obtained. (**Figure 28**)

2.1.3. Surfactant-directed synthesis

Surfactants can selectively attach onto one of the faces in MOF crystal. This specific adsorption of surfactants blocks its growth in a specific direction, leading to the formation of 2D structures. Polyvinylpyrrolidone (PVP) is a commonly used surfactant in the formation of 2D MOF, which can serves as a capping ligand and preferential bind to the [010] plane. Thus, the growth on that facet is prohibited, leading to a 2D structure instead of 3D. Zeng *et al*. reported the formation of 2D Cu MOF through the reaction of Cu_2O and 1,2,4-BTC ligand in the presence of PVP.[60] The coordination topologies of the MOF in the presence of PVP is different from HKUST-1 that is a 3D MOF prepared with the same ligands only. In this case, BTC is partially deprotonated that only two carboxylate groups are involved in the coordination with two discrete

Cu^{2+} ions in monodentate mode. Hence, a polymeric zigzag chains are formed and are connected *via* weak intermolecular interactions including hydrogen bonding, π-π stacking, and van der Waals force to give a nanosheet morphology.

PVP can also be used to control the thickness of 2D MOFs. Zhang *et al*. reported the PVP-directed formation of 2D Co MOF using TCPP and bpy as building blocks (**Figure 29**).[61] They have shown that the thickness of MOF can be controlled by the amount of PVP used. Similar results for 2D Zn–TCPP MOF were reported by Gao *et al*.[62] Fang *et al*. also reported that the reaction of 4,4‴,4⁗-nitrilotris[1,1′-biphneyl]-4-carboxylic acid (NBB) and Zr^{4+} ions in the presence of trifluoroacetic acid (TFA) and PVP yields a 2D Zr MOF with the control of thickness between 6.0 and7.5 nm.[63]

2.1.4. Growth on a solid support

Similar to the surfactant-directed synthesis, growing MOF on a solid-support can also direct the formation of MOF into a 2D structure. Gu *et al*. reported the formation of homochiral 2D Cu MOF, using Cu^{2+} ions, (1R, 1S)-(+)-camphoric acid, and bpy, on different Au substrates functionalized with different self-assembled monolayers (SAMs) of specific orientation and different chirality.[64] The SAMs on Au substrate can guide the formation of 2D Cu MOF, either along the [001] or [110] direction by using OH- and COOH-terminated substrates, respectively. With OH-terminated substrates, the OH groups coordinate with the empty axial sites of paddle-wheel Cu SBU. Further coordination with the camphoric acid and bpy results in the formation of thin 2D MOF film along the [001] orientation. On the other hand, substrate with COOH-terminated functional groups coordinated with the Cu SBU in bidentate bridging μ_2-$\eta^1\eta^1$ mode, thus results in the formation of 2D MOF along the [110] direction.

By employing a suitable solid-support, 2D MOFs can be grown vertically as well. Zhang *et al*. has recently shown that the reaction of H_2bdc and Ni^{2+} ions in the presence of carbon nanowalls (CNW) can vertically grow 2D Ni MOF on CNWs.[65] (**Figure 31**). Chen and co-workers also reported the vertical formation of 2D bimetallic MOF on Ni form *via* the reaction of 2,6-naphthalenedicarboxylic (NDC) acid dipotassium, $Ni(OAc)_2$, and $Fe(OAc)_2$.[66] In the framework structure, NDC coordiates with two metal ions, either Ni^{2+} or Fe^{2+}, in monodentate coordination mode using carboxylates groups to afford the formation of 2D MOF with alternating NDC and MO_6 layers.

2.1.5. Synthesis by decomposition

Since the structure of MOFs is based on non-covalent interaction and weak intermolecular forces, it is easy to decompose when external force, either chemical or physical, is applied. Controlled decomposition of 3D MOFs can yield 2D structured MOFs. Kaskel *et al*. reported that 2D Cu MOF can be obtained by the de-amination of its 3D structure.[67] In the bulk structure, the 2D Cu MOF layers are connected by alkylamine groups *via* hydrogen bondings. Removal of the alkylamine through de-amination process break the weak interlayer interactions and separate them into stabilized single layers (**Figure 34**).

Physical methods, such as ultra-sonication and grinding, are also reported to transform 3D MOFs to 2D MOFs.[68, 69] Grey *et al*. reported the transformation of hexangonal 3D Hf frameworks into 2D MOF nanosheets by grinding or sonication. In its 3D structure, the single layers in Hf MOF have 4,4′-bdc ligands coordinated with four Hf^{2+} ions from $Hf_{12}O_8(OH)_{14}$ cluster in bidentate bridging μ_2-$\eta^1\eta^1$ mode, which stack together in ABBA configuration *via* π-π stacking interaction. Due to unstable nature of stacking, 4,4′-bdc ligands are lost after a period time and the

3D configuration is transformed into a staggered layers, which can afford 2D MOFs upon grinding or sonication.

2.2. 2D covalent-organic framework (2D-COF)

COFs is a porous and crystalline material that is constructed based on the formation of reversible covalent bonds between organic building blocks through reactions such as imine formation, boronic acid condensation, and esterification. Similar to MOFs, COFs also consist of well-defined, versatile, and predicable network, however, COFs have advantages over MOFs in some aspects. In terms of the density, COFs are usually much lighter than MOFs as they are only made of light elements such as carbon, hydrogen and nitrogen. Moreover, it shows higher resistance to air and solvents since it is assembled by covalent bonds.

Recently, the development of COFs has become of great interest because of their customizable functionalities *via* topological design,[70] which endows good potentials in various applications including gas storage, catalysis, optoelectronics, and electrochemical energy storage.[71] In the view of application, 2D COF is more attractive than 3D COFs. The intrinsic π-stacking between layers in 2D COFs can accelerate the transfer of charge carrier which can contribute to the enhanced conductivity and electroactivity.[72] By choosing electroactive building blocks, such as porphyrin, phthalocynine, pyrene, tetrathiafulvalence, and thiophene derivatives, degree of electronic coupling between layers may be tuned *via* various stacking patterns, for example, eclipsed, staggered, serrated, and inclined.[73]

Different from 2D MOFs, the construction of COFs is purely based on the self-assembly approach. Parameters including size, symmetry, connectivity, and coordination angle of the building blocks predefine the network geometry and dimensionality of the framework. In addition, the diversity of building blocks allows tunable pores size and structure in COFs, as well as desired

functionalities. For 2D COFs, building blocks with complementary coordination angles is the key to the formation of an extended sheet with defined pores. **Table 2** shows various ligands of different coordination angles used in the synthesis of 2D COFs. Generally, the construction of 2D COFs can be regarded as a result of the connection between nodes and linkers, which resembles the construction principle of MOFs. Linkers are building blocks in linear shape with coordination angles of 180°, while the nodes are building blocks with various coordination angles of 60°, 90°, 120°, 180°, or a mixture of them, and choices of linkers is determined by the desired function of resulting COFs.

2.2.1. Aromatic building blocks for the control of pore size and structure

At the early stage, the application of COFs has mainly focused on gas storage, and host-guest chemistry. In this case, optimization of the crystallinity, pore structure and size, and stability towards air and moisture are the main development focus. To ensure the crystallinity of the COFs, aromatic building blocks with planar structure are used for better packing between the single layers of COFs, guided by the π-π stacking interaction.[74] Dichtel *et al*. revealed the growth process of a 2D COF based on terephthaldehyde (PDA) and 1,3,5-tris(4-aminophenyl)benzene (TAB). Initially formed amorphous network was crystallized in the layered 2D network stabilized by π-π stacking interactions.[74] The pore structure and size in COFs is determined by the coordination angles and length (*i.e.*, numbers of aromatic rings) or alkyl substituent of the building block, respectively. COFs with hexagonal pores is the most commonly reported, which is resulted from the combination of linear linkers and 120° nodes.[71, 74-85] For example, Yaghi *et al*. reported a 2D COF structure composed of 2,5-diethyoxyterephthalohydrazide (DETH) and 1,3,5-triformylbenzene (TFB), which has hexagonal pores with diameter of 2.8 nm.[77] By replacing

TFB with 1,3,5-tris(4-formylphenyl)benzene (TFPB), with one more benzene inserted between the aldehydes and central benzene, the diameter of hexagonal pore was increased to 3.5 nm.

Lavigne *et al*. also reported 2D COFs with controlled pore sizes, which was obtained by the condensation of benzene-1,3,5-triboronic acid and various dialkyl substituted derivatives of 1,2,4,5-tetrahydroxybenzene (THB) (**Figure 3b**).[71] The incorporation of alkyl substituents of different lengths changed the pore diameter, and thus the absorption properties of the resulting COFs could be tuned. Another report by Yan *et al*.[78] demonstrates the size tenability of 2D COFs. They carried out the imidization reaction of pyrometalltic dianhydride (PA) with various sizes of anilines, including 1,3,5-tris(4-aminophenyl)benzene (TAB), 1,3,5-tris[4-amino(1,1-biphenyl-4-yl)]benzene (TABPB), and tris(4-aminophenyl)amine (TAPA), and obtained similar 2D COF structures, stacked in serrated configuration, of different pore sizes, with the largest one being 42×53 Å^2.

The rectangular or square pores in 2D COFs can fabricated by combining linear linkers with 90° nodes.[86, 87] Zheng *et al*. reported a 2D COF with rectangular pores with a brick-all topology based on imine condensation between T-shaped building block, 4,4′,4″-(1*H*-benzo[*d*]imidazole-2,4,7-triyl)tribenzaldehyde (BIBA), and 1,4-diaminobenzene (DAB).[87] The boronic esterification of Zinc(II)(2,3,9,10,16,17,23,24-octahydroxyphthalocyaninato) ([Zn(Pc(OH)$_8$)]) and 1,4-benzenediboronic acid (BDBA) also lead to the formation of 2D COF with square grid structure. It is interesting to note that the solvents used in those reactions exert a strong effect on the nucleation, polymerization, and crystallization process of the COFs.[86]

Mixed pore types in a 2D COF can be designed by using ligands with special geometry.[88-91] For example, McGrier *et al*. reported the formation of 2D COFs based on the condensation reaction of a linear linker, 1,4-benzenediboronic acid (BDBA), and dehydrobenxoannulenes[12]

(DBA[12]), a building block of 120° coordination angle.[88] DBA[12] is a conjugated monocyclic ring with a triangular structure, which affords the 2D COF with two types of pore structures. The triangular pores are originated from DBA itself and the other hexagonal pores are created by the condensation between building blocks (**Figure 3d**). Each single layer is stacked on the neighboring layer in eclipsed configuration. The sizes of both triangular and hexagonal pores can be tuned by extending the length of alkynyl units in DBA[12] to DBA[18], which allows a periodic crystalline 2D network with largeer surface area. Similar COF structure is reported by Bein and co-workers[90] who used a linear liner, benzo[1,2-b:4,5-b′]-dithiophene-2,6-dicarboxaldehyde (BDDA), with 4,4′,4″,4‴-(ethene,1,1,2,2-tetrayl)tetraaniline (ETTA) for imine condensation. ETTA contains two different coordination angles, 60° and 130°. Therefore, the resultant star-shaped COF contains two type of pores with triangular and hexagonal shapes. An exceptional case was reported by Zhao *et al*. that building blocks of 120° angle has been used for the formation of COF.[89] They found out that the condensation reaction of non-planar building blocks, tris(4-aminophenyl)amine (TAPA), and planar building blocks, 4,4′,4″,4‴,4⁗,4⁗′-(dipyrazino[2,3-*f*:2′,3′-h]quinoxaline-2,3,6,7,10,11-hexayl)hexaaniline (PQHHA), produces a 2D COF containing rhombous pores of different sizes. Interestingly, the imine bond can adopt either heterodromous or homodromous orientation, hence two different COFs are possible. The COFs with imine bonds in homodromous orientation would grow as an amorphous polyimine material with disordered internal structure.

2.2.2. The imine linkage of aromatic building blocks with C_3-symmetries

One of the characteristic features of 2D COFs is the high surface-to-volume ratio. This allows their application in chemical transformation and sensing. 2D COFs constructed with C_3-symmetric aromatic ligands as nodes usually provide large specific surface areas with high porosity, and thus

can provide more active sites accessible for the substrates, making them suitable for sensing and chemical transformation applications.[82, 92-96] In addition, the framework structure built by imine linkage is more preferable, as the imine N atoms can either coordinate with metal ions to act as catalytic site, or interact with analytes for sensing application through weak intermolecular forces. For example, Wang *et al*. reported that a Pd-dopped 2D COF prepared by the imine condensation reaction between TFB and 1,4-diaminobenzene DAB shows a good catalytic activity in Suzuki-Miayura coupling reaction.[92] The single layer of this COF is comprised of the hexagonal pores with eclipsed imine bonds, and the layers are staged together to yield a 2D network structure through the stabilization by the π-π stacking interactions between adjacent layers. Through a simple post-treatment with $Pd(OAc)_2$, Pd^{2+} ions were coordinated to the imine N atoms to result in a Pd-dopped COF. They explained that the large specific surface area of this COF gives easy access of substrates to the active site and fast diffusion for the bulky products. Another interesting example was given by Han and co-workers.[93] Through the [3+3] imine condensation reaction between non-planar C_3-symmetry building blocks, TAPA and tris(4-formylphenyl)amine (TFPA), they constructed a 2D COF single layer with hexagonal pores, which stacked together *via* hydrogen bonding in eclipsed configuration due to flexible non-planar building blocks. As a result, this bulk COFs can be easily exfoliated into ultrathin 2D nanosheets by ultrasonication. The resulting nanosheet provides ultrahigh surface area which can act as a fluorescence sensing platform for the highly sensitive and selective detection of DNA, owing to the hydrogen bonding between imine N atoms and DNA.

2.2.3. Highly conjugated aromatic building blocks

The construction of 2D COFs based on the planar aromatic building blocks allows the single layers to stack each other *via* π-π stacking, of which eclipsed mode between layers is the most

commonly observed. Such eclipsed stacking in 2D COF induces unique properties such as excimer emission and exciton migration, thus endows or facilitates the luminescent properties of the material. Besides, eclipsed stacking can also accelerate or direct the transfer of charge carrier *via* the π-conjugated tunnel, leading to the enhanced conductivity and electrocatalytic activity. These properties have sparked vast investigations exploring the application of 2D COFs in optoelectronic and energy conversion storage. For these applications, it is most important to construct 2D COF based on redox active building blocks. Conjugated building blocks with redox behavior, which contains heterocycles such as pyridine and triazine in the building block skeleton, are one of the types that have been widely used.[97-99] Bhaumik *et al*. reported a Schiff base condensation of triformylphloroglucinol (TFP) and 1,5-diaminonaphthalene (DAN),[99] in which the stacking of 2D COF single layers in eclipsed configuration afforded a 2D network (**Figure 3e**). Good supercapacitive property observed has been attributed to the π-conjugated porous channel-like network that allows proton diffusion, the redox activites of N atoms on the building blocks, and the high specific surface area of the material.

Another type of well-studied building blocks is the molecules with fused ring moieties, including pyrene and triphenylene which are polycylic aromatic hydrocarbon.[70, 100-103] The planar structure of this type of building blocks can direct the eclipsed stacking of the resultant 2D COF single layers *via* π-π stacking interaction between the aromatic rings. In addition, both pyrene and triphenylene are luminescent molecules with semiconducting properties. Therefore, 2D COFs constructed based on this type of building blocks are expected to show enhanced luminescent and semiconducting properties. Jiang *et al*. reported that a condensation reaction of 2,3,6,7,10,11-hexahydroxytriphenylene (HHTP) and pyrene-2,7-diboronic acid (PDBA) forms a belt-shaped luminescent and seminconducting 2D COF. The alternate linkage between pyrene and

triphenylene functionalities led to the formation of the single layer of the COF with hexagonal pores (**Figure 3f**).[70] The layers are stacked in eclipsed configuration to form a highly-ordered network structure with the stabilization *via* π-π stacking interactions. Because of the highly ordered structure, the material is highly luminescent, and the photon harvest in a wide range of wavelength is possible. Besides, as it is an electrically conductive material due to the π-conjugated channels, this material can carry out a repetitive on-off current switching at room temperature, and makes it a potential candidate for optoelectronic application. A similar approach was taken by Dong *et al*. to prepare a thermoelectric 2D COF using 2,7-diaminofluorene (AF) and TFB.[103] The presence of fluorene moiety in the single layer formed endows good electronic charge-transfer properties, which could be further enhanced by iodine doping.

Building blocks containing heterocyclic macrocycle moieties, such as phthalocyanine[72, 104-107] and porphyrin,[73, 108-112] are the most popular in the 2D COF synthesis. In addition to their highly order structure and light harvesting capability, the most interesting features of this type of ligands is their ability of coordinating metal ions with the N atoms of hetero-macrocyclic rings, which allows the formation of a metal-doped 2D COFs. Dichtek *et al*. reported the formation of 2D square grid COF structure *via* $BF_3 \cdot OEt_2$-catalyzed boronate esterification of phthalocyanine tetra(acetonide) (PCTA) and BDBA.[72] The phthalocyanines stack in an eclipsed configuration within the COF gives the stabilization by π-π stacking interactions. This 2D COF shows a broad absorption of the solar spectrum, efficient charge-transfer throughout the stacked phthalocyanines, and good thermal stability. Seki *et al*. also reported the condensation between [Ni-($Pc(OH)_8$)] and 1,4-benzothiadiazole diboronic acid (BTDBB), which afforded an *n*-type seminconducting 2D COF (**Figure 3g**).[104] In the framework structure, the single layers stack together with benzothiadiazole to benzothiaidzole and phthalocyanine to phthalocyanine, in an eclipsed

configuration due to π-π stacking interactions. The integration of an electron-withdrawing benzothiadizaole unit in the framework leads to the drastic changes in the carrier-transport mode and switches it to an electron transporting framework instead of a hole-transporting skeleton. The eclipsed stacking of phthalocyanine provides a conductive channel for carrier transport, endows efficient absorbance over a wide range of wavelength, from visible to near-IR region up to 1000 nm, and exhibits excellent electron-transporting properties.

Bhattacharya *et al*. reported the Schiff-base type condensation between 5,10,15,20-tetrakis(4-aminophenyl)porphyrin (TAPP) and 1,3,6,8-tetrakis(4-formylphenyl)pyrene (TFFP) to afford a crystalline 2D COF (**Figure 3i**).[73] The single layers consist of alternative imine linkage between porphyrin and pyrene units to form square pores. Theses layers are stacked in an eclipsed configuration which is stabilized by π-π stacking interaction to build up a 2D network with moderate surface area and chemical stability. The pyrene-based conducting channel was observed to facilitate the electron transfer. It is of interest to note that this 2D COF can conduct metal-free hydrogen production in acidic media. This was attributed to the imine N atoms which is the active center for the reaction. Jiang *et al*. also reported another 2D COF based on Zn-TDHPP and squaric acid (SA).[109] According to the simulation, the resultant single layer has a zwitterionic structure that allows resonance conjugation between porphyrin and SA units. The zigzag structure of single layer was further extended through the polymerization to form a flat and twisted 2D layer structure with bowl-shaped pores. The resulting electron-deficient skeleton can allow the electron flow through the stacked column and over the 2D plane, thus enhances the light-harvesting capacity. More recently, Yaghi *et al*. reported the reaction of Co–TAPP with linear linkers, including BDA, 2,5-dimethoxyterephthaldehyde (DMTPA), 2-fluoroterephthaldehyde (FTPA) or 2,3,5,6-tetrafluoroterephthaldehyde (TFTPA), for the formation of oriented thin films on glassy carbon

electrode.[112] The electrode coated with the COF was applied in the study of electrocatalytic CO_2 reduction. The incorporation of catalytically active Co site in the framework successfully tuned the electronic properties of the COF to function as active electrocatalyst for CO_2 reduction to CO at low overpotential with high selectivity under high current density.

Table 2. Ligands of different coordination angles used in the synthesis of 2D COF.

3. Applications

Owing to their 2D structures, 2D-MOFs/COFs feature unique physical and chemical properties such as high conductivity, large surface area, and ultrahigh porosity that can be easily modulated.[113-116] By changing the combination of metal nodes and organic ligands, versatile structures and thus functions can be achieved with MOFs to meet specific application needs. The organic building units connected *via* strong covalent bonds in COFs offer lightweight porous structures that can be tuned by altering the type of building units. Nowadays, both 2D-MOFs and COFs are mainly used for gas separation/storage, nanofiltration, catalysis, electrocatalysis, energy storage (batteries, supercapacitors), and sensing. In this section, we will focus on the use of 2D-MOFs and COFs in energy-related applications and discuss in view of their structure-property relationships. Although many recent publications involve 2D-MOFs/COFs in the developments of energy-related applications, it should be noted that the reports merely using 2D-COFs/MOFs as a precursor for other materials, such as carbon[59] and metal oxides,[117] are beyond our discussion here.

3.1. Molecule separation and storage

3.1.1. Separation

Separation is a critical process in the chemical industry, especially those closely related to the energy production and environmental pollution control, such as H_2 purification (H_2/N_2, H_2/CO_2, H_2/CO, *etc.*), air separation (O_2/N_2), CO_2 separation (CO_2/CH_4, CO_2/N_2, *etc.*), hazardous substance removal, and valuable products separation (C_3H_6/C_3H_8, C_2H_4/C_2H_6, *etc.*). Selectivity and permeability towards specific molecules are considered as the most important factors in evaluating the separation performance. Selectivity, quantified by the separation factor (SF), is controlled by the pore aperture and pore distribution of membranes. Contrarily, the larger pore aperture usually

results in the higher permeability. Although MOFs and COFs have already shown the separation ability, a higher permeability and selectivity fulfilling the industrial standard is still appreciated.[118, 119] To achieve this, an ultrathin 2D structure with evenly distributed and tunable pores are highly desired,[120] making 2D-MOFs and COFs the ideal candidates for separation. A computational study by Zhong *et al.* demonstrates a few-layered ultrathin COFs structure showing high CO_2 flux and high CO_2/N_2 selectivity, far above the Robeson's upper bound.[121] Recently, development of nanosheets and membranes consist of 2D-MOFs or 2D-COFs for separation has been gaining decent attention.[39, 122, 123]

For gas separation, the kinetic diameter of gas molecules (0.25−0.5 nm)[124] is smaller than the pore aperture of COFs (typically 0.8−5 nm)[125]. For selectivity improvement, significant efforts have been made to decrease the pore aperture using different strategies, such as pore modulation[126] and hybridization[127, 128]. Caro and co-workers constructed a bilayer membrane using imine-linked COF-LZU1 (pore aperture = ~1.8 nm) and azine-linked ACOF-1 (pore aperture = ~0.94 nm).[129] The interlaced pore aperture is similar to the kinetic diameter of gas molecules, resulting in a highly selective H_2 separation (H_2/CO_2, H_2/N_2, and H_2/CH_4). Despite the development of 2D-COFs, its selectivity over gas separation is still generally poor compared to those of 2D-MOFs of which pore apertures are typically smaller than 1 nm.[124, 130] As a result, there are currently more examples reported using 2D-MOFs for gas separation, especially for H_2 and CO_2 separation.[39, 131, 132] In 2014, Yang and co-workers reported an ultrathin molecular sieve membrane built with 2D-MOFs ($Zn_2(bim)_4$, bim=benzimidazole, thickness = ~1 nm, **Figure 1a**), which has a pore size of 0.21 nm (**Figure 1b** and **1c**) and shows an ultrahigh H_2/CO_2 selectivity (>200) and an unusual proportional relationship between H_2 permeance and H_2 selectivity.[131] By converting rigid 3D MOFs to flexible 2D MOFs, Webley *et al.* reported an

enhanced selectivity towards CO_2/N_2 and CH_4/N_2 separation.[133] To increase the selectivity and permeance towards gas mixture, 2D/ultrathin hybrid materials consist of MOFs and other components are also developed, such as graphene,[134, 135] COFs,[127] ZnO,[136] and polymeric matrices,[137, 138] which act as either a template to assist the 2D shape or a pore controller.

In addition to the gas separations, 2D MOFs are also widely used to separate larger molecules.[139, 140] For example, a size-selective 2D-MOF made of iron porphyrin complex interconnected with divalent metal ion have demonstrated a >90% rejection rates for organic dye with a size larger than 0.8 × 1.1 nm, while maintaining the ultrahigh permeance of 4,243 L m^{-2} h^{-1} bar^{-1}, two times higher than the commercial polymeric nanofilteration membrane.[141] An interesting finding was recently reported by Ruoff *et al.* which shows that 2D Cu-MOFs can be used for the size-selective separation of gold nanoparticles, demonstrating the significant potential of 2D-MOF materials.[36] Sharing the similar tunable pore properties to MOFs, 2D-COFs are employed for separation and filtration as well. Linked *via* covalent bonding of organic blocks, 2D-COF materials possess different binding sites and pores for selective interaction of molecules.[142-144] Jiang and co-workers reported a 2D-COFs consist of 1D open channels for the removal of iodine from toxic vapor.[145] A recent example reported by Hu *et al.* demonstrated that 2D-COF is capable of separating arylenevinylene macrocycles from their linear polymer analogs after cyclooligomerization process.[146] As shown in **Figure 1c** and **1d**, the as-prepared COF can host AVM2 (arylenevinylene macrocycles with $COOC_{10}H_{21}$ functional groups) and rejects the linear by-products. The AVM2 can be easily seperated after solvent treatment. In another report, Rosei *et al.* showed that a single-layer COF (COF-1) could even act as a host architecture for C60 fullerene molecules by merely dipping the COF material into the fullerene solution.[147]

3.1.2. Gas storage

Gas storage, mainly targeting CO_2 and H_2, is of great interest due to its significance in greenhouse gas reduction and development of non-carbon energy sources. Due to the high surface area and inimitable porosity, both MOFs and COFs have attracted tremendous attention.[148, 149] Generally, 2D-MOFs/COFs with larger surface areas possess higher CO_2 and H_2 uptake capacities under the same conditions, and various framework materials have been developed based on size/shape exclusion and adsorbate–surface interactions between sites and gas molecules.[124, 125, 150] Until now, more reports are available for 2D-MOFs than 2D-COFs, that demonstrate the application for CO_2 and H_2 storage owing to their smaller pore size and large pore volume.[151-153] 2D-MOFs possess both organic molecule and metals sites that can be tuned to fabricate materials with desired pore structure.[119]

Extensive studies have been focused on the mechanism of CO_2 adsorption behavior in 2D-MOF layers due to its environmental importance.[154, 155] On one hand, openly accessible Lewis basic sites located in the channels of 2D-MOFs are considered as the key for CO_2 binding and capture, which leads to the development of nitrogen-containing ligands and the bonding metal ions (mainly Cu, Zn, Co) in pursuit of Lewis basic sites control.[156-159] For example, by surface functionalization using amino groups, Zhang *et al.* showed that the CO_2 uptake of 2D Cu-MOFs rises to 78.3 mg g^{-1}.[160] Functions such as selective gate adsorption of CO_2 *via* a dynamic pore-opening/pore-closing processes can also be achieved using 2D Cu-MOFs and guest molecules.[161] The geometry of MOF channels, on the other hand, is critical for high volume CO_2 update.[162] Rao and co-workers demonstrated that a 2D graphene-Cd-MOF composites show the stepwise CO_2 uptake with a large hysteresis compared to a single-step process of the pristine MOF.[163]

Various 2D-COFs have been also studied for CO_2 and H_2 storage theoretically[164] and experimentally[165-167] owing to their high-aspect-ratio features. Compared to boronate-based COFs, the imine-linked COFs are more stable under various conditions, including heat and moisture.[168] For example, an azine-linked 2D-COF (ACOF-1) with a high surface area (>1,000 $m^2 g^{-1}$) and small pore size stores up to 177 mg g^{-1} of CO_2, 9.9 mg g^{-1} of H_2 at 273 K and 1 bar.[169] The authors attributed such good performances to the accessible nitrogen active sites in small pores, which can bind CO_2 molecules and trap smaller gas like H_2.

3.2. Energy conversion

Due to their ultrathin thickness and high surface-to-volume atom ratios, abundant exposed catalytic sites can be found on the surface and in the tunnels of 2D materials, including both 2D-MOFs and 2D-COFs. Such features are of great benefit for the composites consist of 2D-MOFs/COFs and other components in applying to various energy conversion reactions, such as heterogeneous catalysis, photocatalysis, and electrolysis. The composites based on 2D MOFs/COFs usually show a much enhanced performance compared to their bulk siblings.[47, 60, 62, 170-174] In this section, the energy conversion related applications of 2D-MOFs/COFs, including CO_2 reduction reaction (CO_2RR), water-splitting reaction, and oxygen reduction reaction (ORR), are discussed and summarized.

3.2.1. CO_2 conversion (CO_2RR)

Apart from the capture of CO_2 molecules, the conversion of CO_2 to the value-added chemicals, such as CO, formic acid, methanol, ethanol, and the other higher carbon molecules, is another adopted route for greenhouse gas reduction. This approach not only eliminates CO_2 from the atmosphere but also provides alternative sustainable and clean energy sources. Among the various approaches used/combined to promote the CO_2RR, namely homogeneous catalysis, heterogeneous

catalysis, and electrochemical catalysis, currently the electrochemical reduction of CO_2 is considered to be the most energy efficient and clean methods.[175] For years, studies have been focused on the rational design of electrocatalysts with excellent Faradic efficiency and good product selectivity. Numerous potential electrocatalyst materials, including metals, metal oxides, metal complexes, organic molecules, and polymers have been explored.[175-177] Demonstrated in a series of impactful papers,[178, 179] the application of MOFs and COFs in CO_2 conversion has started to receive the spotlight since 2014. A recent review by Yaghi *et al.* summarized the current advances of CO_2 storage and conversion using MOFs.[180]

More recently, the composites based on the 2D-MOFs and 2D-COFs are gaining more and more attention. Their higher charge carrier mobility and lower resistivity associated with 2D morphology have been extensively reported accompanying the hunt for new 2D-MOFs/COFs,[114, 181, 182] and such features make both 2D-MOFs/COFs the promising candidates for electrocatalysis.

One of the advantages of 2D-MOFs and 2D-COFs for CO_2RR is that the discrete frontier orbitals of organic linkers can interact with CO_2 molecules in specific orientations for high selectivity. However, the guest metal sites/surface are essential for efficient electron transfer to promote CO_2 conversion. In 2018, by introducing cobalt porphyrin units to COFs (**Figure 2a**), Yaghi *et al.* reported a series of electrochemically stable 2D-COF (COF-366-Co and COF-366-F-Co, **Figure 2b**) nanosheets with a reticular structure for CO_2 to CO reduction with a low overpotential (550 mV *vs.* reversible hydrogen electrode (RHE)) and high selectivity (Faradaic efficiency = 87%) at high current densities (65 mA mg^{-1}, **Figure 2c**), which is better than the corresponding molecular catalysts and bulk samples.[183] The authors attribute such excellent performances to the molecule-level control of catalytically active cobalt sites *via* facile

functionalization of the reticular structure with electron-withdrawing groups. In another report by Deng and co-workers, COF materials in both 2D and 3D morphologies are prepared and coated on the Ag electrode (**Figure 2d**).[184] As shown in **Figure 2e**, the abundant amino groups in the backbone can form carbamate intermediates at the Ag/COF interface and facilitate the CO_2RR, achieving a CO_2 to CO Faradaic efficiency of 53% at -0.70 V and 80% at -0.85 V (*vs.* RHE, **Figure 2f**).

Notably, CO_2 conversion using 2D-COFs/MOFs is not confined to the electrochemical approaches but also includes the heterogeneous catalysis and photocatalysis. For example, Sun and co-workers recently reported an ultrathin 2D Zn porphyrin-based MOF for selective photoreduction of CO_2 to CO.[62] Compared to the Zn-MOF bulk, 2D structure of MOFs demonstrates a better conductivity and longer lifetime of the photogenerated electron-hole pairs. Another example reported by Suresh *et al.* shows that a 2D Zn-MOF material can act as a highly active, solvent-free, binary catalyst for CO_2 cycloaddition with epoxides under ambient conditions (1 atm and room temperature), realizing the minimum energy utilization for CO_2 conversion.[185]

3.2.2. Hydrogen evolution reaction (HER)

H_2 is the most promising energy source to replace current carbon-based fuels. However, its high-cost for mass production is one of the main drawbacks hindering its industrialization. Currently, water-splitting is considered as one of the most energy-efficient methods to enable large-scale H_2 production. The two half-reactions of water-splitting reaction, namely hydrogen evolution reaction (HER) and oxygen evolution reaction (OER), are targeted as the primary challenge and widely studied respectively in the recent decades. Although high efficiencies (high Faradaic efficiency and low overpotential) of both reactions have been realized using noble metals and their metal oxides as electrocatalyst or photocatalyst, cheap and non-precious materials are

preferred due to the cost and availability issues. Given that, the development of MOFs, COFs, and their derivatives have provided a new family of catalysts with nearly infinite combinations for rational catalyst design.[177, 186] Among them, ultrathin 2D materials, including 2D-MOFs/COFs, are the latest candidates that have been employed for both electrocatalytic and photocatalytic water splitting.[187]

Electrocatalytic HER, involving the electrons transfer from the electrode to active sites and the proton transfer from the environment to active sites, requires high electronic and protonic conductivity, high stability under the acidic/basic condition, and high electrochemical surface area, which can be fulfilled by tailoring 2D-MOFs/COFs. The metal nodes in MOFs can be used as the active site for HER, as shown by Marinescu and co-workers.[44] In 2014, they described one of the earliest examples of using cobalt-containing 2D-MOF materials (structure shown in **Figure 3a**) as a cathode for hydrogen evolution from water, with the overpotential of 0.34 V (Co-benzenehexathiol) and 0.53 V (Co-triphenylene-2,3,6,7,10,11-hexathiol) *vs.* standard hydrogen electrode (SHE) at 10 mA cm^{-2} in pH=1.3 (**Figure 3b**). They attributed such high activities to the high atomic catalyst loadings and remarkable stability under acidic conditions. Later on, the same group explored the thickness factors of MOFs (Metal = Co, Ni, Fe, **Figure 3c**).[188] They found out that both charge and proton transfer are blocked at a thickness over ~1 μm (**Figure 3d**), showing the advantage of ultrathin morphology. The best HER performance in their study was achieved by using Co other than Ni and Fe. In 2015, using a "bottom-up" approach, Feng *et al.* fabricated a large-area and free-standing Ni-MOF (Ni-triphenylene-2,3,6,7,10,11-hexathiol, structure is shown in **Figure 3e**) with a single-layer structure.[189] This 2D Ni-MOF showed an overpotential of 413 mV (*vs.* RHE) at 10 mA cm^{-2} in pH=1.3 (**Figure 3f**), which is better than previous reports used the same organic linker. The advantages of using 2D-COFs/MOFs

possessing high stability and electronic and protonic conductivities have been well demonstrated by the above examples. In addition to altering the metal species, the electronic surrounding of the metal sites can also affect the HER activity. In another report by Feng's group, they selectively changed the coordination environments of the metal sites (Co and Ni) in 2D-MOF from MS_4 to MS_2N_2 and MN_4.[52] A fascinating activity trend of MS_2N_2>MN_4>MS_4 was established and the 2D Co-MOF with MS_2N_2 coordination type exhibited an low overpotential of 283 mV at 10 mA cm^{-2}. Theoretical calculation suggests that the protonation step is preferred at the M-N sites in the MS_2N_2 complexes. However, the metal sites in MOFs are not indispensable. In 2017, Pradhan *et al.* reported a metal-free imine-based conjugated pyrene, porphyrin comprised microporous quasi-2D-COF for electrochemical HER.[190] The imine nitrogen sites of the quasi-2D-COF are proposed as the active sites for proton reduction.

Photocatalytic HER, using solar energy, is another promising route towards energy conversion of H_2O to H_2. The π-π stacking structure and conjugated organic backbonds can absorb photons, leading to the electron jump towards a higher energy molecular orbital, and thus facilitating the charge-hole separation. As the electronic and optical properties of the MOFs/COFs can be readily tuned by tailoring the organic linkers[191-193], photocatalytic properties can be introduced to 2D-MOFs/COFs.[46, 194, 195] Using a visible-light-harvesting anthracene-based bipyridine ligand, Du *et al.* synthesized a new 2D Cu-MOF material with a narrow forbidden-band of 2.13 eV.[196] With triethanamine (TEA) as the hole scavenger, the H_2 evolution amount reaches 75.89 mmol g^{-1} within 18 h irradiation and pH = 12. The authors proposed a similar mechanism comparable to the conventional inorganic semiconductors. In another report worth mentioning, Lotsch *et al.* constructed an azine-based 2D-COF as a photocatalyst support (Pt as co-catalyst) for

photocatalytic HER (1,703 mmol h^{-1} g^{-1}), and the numbers of N atoms can be used to fine-tune the band energy.[197]

Moreover, a new photoelectrocatalytic approach using metal-free 2D-COFs as the photocathode for HER was recently demonstrated by Bein and co-workers.[198] Proving metal sites are not indispensable, they managed to prepare a 2D-COF with a direct band gap of 2.47eV. Such 2D-COF shows great structural and photocurrent stability during the photoelectrocatalytic process, opening up the unexplored potential of using metal-free 2D-COFs for HER.

3.2.3. Oxygen evolution reaction (OER)

OER carries a critical importance owing to its kinetic impact on HER during water splitting and also rechargeable metal-air batteries. Due to the high concentration and single-site distribution of active metal sites, MOFs and COFs have already shown promising results.[199] However, problems similar to many bulk catalysts, such as low charge transport efficiency and low mass permeability, still persist and new problems associated with the stability of COFs/MOFs under acidic/basic conditions have been raised.

Having higher conductivity and stability compared with their 3D counterparts, the COFs/MOFs-based electrocatalysts with 2D/ultrathin morphology on a conductive substrate are suggested to be the solution to the afrementioned problems.[200, 201] Starting from 2016, studies have been focusing on the approaches to lower the overpotential of OER *via* exposing more active sites, increasing the activity of metal sites, and improving the conductivity. Exfoliation of 3D-MOFs to 2D-MOFs is the reasonable way to expose the active sites on the surface, however, it is still challenging. Recently, Zhang *et al.* reported an electrochemical exfoliation method to turn pillared-layer MOFs to ultrathin (2 nm) nanosheets by *in situ* removing the pillar ligands.[202] A

low overpotential of 211 mV *vs.* RHE at a current density of 10 mA cm^{-2} and a Faradaic efficiency of 99% were reported using the 2D Co-MOFs.

Currently, metal doping method is widely used to tune the electronic properties of the active sites. In 2016, Tang and co-workers reported ultrathin NiCo-MOFs (structure shown in **Figure 4a**, thickness = ~3 nm, **Figure 4b**) as a promising electrocatalyst for the OER under alkaline conditions with an overpotential of 189 mV (*vs.* RHE at a current density of 10 mA cm^{-2}) and only 2.6% decay in anodic current after 200 h of continuous electrolysis, as shown in **Figure 4d** and **4e**.[203] The authors attributed the high activity of bimetallic MOFs to the electronic interaction between Ni and Co atoms. Meanwhile, the 2D-MOFs possess more coordinatively unsaturated metal sites (**Figure 4c**) on the surface which facilitate the adsorption of hydroxide groups compared to the bulk bimetallic MOFs. The similar strategy was employed by other researchers to construct NiFe 2D-MOFs[66], NiCo 2D-MOFs[204]. Furthermore, a recent report by our group suggested that the electron transfer in 2D CoNi-MOFs is facilitated along the Z-axis better than the other directions, which can lead to an enhanced catalytic activity of selected planes.[205]

The conductivity of the 2D-MOFs can be improved by the incorporation of conductive layers, as shown by Huang and co-workers.[206] In their studies, $Ti_3C_2T_x$ nanosheets were introduced to 2D-MOFs to form hybrid nanosheets with lower charge transfer resistance of OER (from 118 Ω of 2D-MOFs to 86 Ω of the hybrid nanosheets).

3.2.4. Oxygen reduction reaction (ORR)

Another electrocatalytic application of 2D-MOFs/COFs is the oxygen reduction reaction (ORR), which is the fundamental reaction related to fuel cells and metal-air batteries. Although the commercial Pt-based catalysts show the best performance at present, the high-cost of Pt demands the development of non-platinum group metal electrocatalysts, such as Ni, Cu, and Co.

The ORR mechanism and the structure-activity relationship are yet to be understood. Recently, the attempts to increase the number of active sites and the surface area have led to the development of MOFs/COFs-based catalysts.[177, 207]

Currently, majority of publications reporting the use of 2D-MOFs/COFs merely engage them as the precursors for high surface area carbon and nitrogen-doped carbon supports,[208] which is beyond our discussion here. There are only a few report on the direct catalytic ORR performance of 2D-MOFs/COFs.[209] The distinct, spatially isolated active sites of 2D-MOFs/COFs present the ideal model for mechanism studies and rationalization of catalyst design.[210] For example, in 2017, Dincă and co-workers presented experimental and computational results elucidating the mechanism of ORR using a conductive 2D Ni-MOF, $Ni_3(HITP)_2$, where HITP = 2,3,6,7,10,11-hexaiminotriphenylene.[211] Notably, both kinetic and X-ray absorption spectroscopy (XAS) results suggest that the ligand, rather than the Ni sites, is responsible for O_2 molecule binding.

3.3. Energy storage

Besides gas storage and electrochemical/photochemical conversion, the other two major applications of MOFs/COFs are batteries and supercapacitors. Although most of the studies focus on the inorganic materials and their carbon-involved composites, the organic materials, such as MOFs and COFs, have been gaining increasing attention due to their chemical flexibility, environmental benefit, and cost advantage, as summarised in a recent review paper by Zhang *et al.*[19]. As a new class of 2D porous materials, both 2D-MOFs and 2D-COFs with periodic molecular ordering and exceptional well-defined porosities that can be accessed by electrons and chemical species in various electrochemical environments have been utilized as suitable candidates for energy storage applications, such as batteries and supercapacitors.

3.3.1. Battery

The rapid developments and broad applications of lithium-ion batteries (LIBs), as a current main stream technology for portable electronics and off-grid power systems like vehicles, demand higher specific capacity, higher energy density, and outstanding stability. Conductive 2D-MOFs/COFs are considered as potential alternative candidates for Li storage due to their distinct layered and porous structures compared to their inorganic analogs, like graphene. As stated previously, vast efforts to prepare carbon materials using 2D-MOFs/COFs for battery application can be found elsewhere.[212, 213]

For conductive 2D-COFs, the stacked interlayer functional π-electron systems interacting with maximal π-orbital overlap *via* van der Waals interaction makes them ideal for charge transport while exhibiting open porous channels that run parallel to the direction of stacking.[214] Such unique features enable the 2D-COFs to store Li while maintaining high electronic conductivity along the π-electron systems, as demonstrated in a paper by Li and co-workers.[215] In their study, a 2D-COF-based polyporphyrin film was shown as one of the first examples of using 2D-COFs as new anode materials in LIBs, with a reversible LIB capacity up to 666 mAh g^{-1}. The authors emphasized that the finely eclipsed alignment of 2D polyporphyrin sheets favor carrier flow over the frameworks, resulting in high electronic conductivity. Meanwhile, the 2D structure of COF provides sufficient internal Li-insertion channels for Li atom adsorption and short-ended path for fast Li ion diffusion. However, due to the strong π–π interactions between 2D-COF layers, especially in an eclipsed stacking, it becomes more difficult for the Li ions to diffuse into the deeply buried interior active sites during cycles. Given that, hybrid materials consisting of 2D-COFs and other conductive/porous materials are proposed. For example, Wang *et al.* reported a hybrid composite including 2D-COFs and carbon nanotubes (CNTs) as the anode material for LIBs, as shown in **Figure 5a** and **5b**.[216] A stable reversible capacity of 1,021 mAh g^{-1} has been

achieved after 320 cycles, and the lifetime of LIBs are much longer than using 2D-COFs only. The authors proposed a mechanism with 14-lithium-storage for a COF monomer (one Li ion per C=N group and six Li ions per benzene ring) to explain such a high capacity (**Figure 5c**), and the long lifetime has been attributed to the ultrathin morphology and high conductivity of CNTs.

Similar to 2D-COFs, conductive 2D-MOFs (mainly dithiolene-based MOFs[114]) are also being gradually employed as the anode/cathode materials for batteries. However, owing to the nature of coordination bonding, two of the major problems associated with MOFs is the stability of the framework during the charge/discharge processes and the conductivity of the frameworks of 2D-MOFs. Loh and co-workers provided an approach to increase the stability by changing the metal node to increase the bonding strength.[217] The reported 2D Cd(II)-MOFs showed a greater stability and higher capacity compared to its Co(II)-MOF analog. Choosing an electrochemically stable organic ligand is another way to increase the stability of 2D-MOFs, and recently redox-active ligands have shown promising performances by many researchers. Kimizuka *et al.* reported the first example of using phthalocyanine-based 2D Cu-MOFs as the cathode of LIBs.[49] The authors demonstrated a high thermal and electrochemical stability of the materials, showing an electrical conductivity of 1.6×10^{-6} S cm^{-1} at 80°C and a charge/discharge capacities of 151/128 mAh g^{-1}. In another report, Bao *et al.* described a 2D Co-MOF as anode material for Na ion batteries with hexaaminobenzene (HAB) as the organic linker for the first time.[218] With the use of HAB molecules that show a reversible three-electron redox reaction per molecule, high thermal and chemical stability, surprisingly high conductivity of 1.57 S cm^{-1}, and specific capacity 291 mAh g^{-1} have been demonstrated. The similar strategy of constructing redox-active yet stable 2D-MOFs as the electrode material was used in other studies as well. Recently, Nishihara *et al.* showed a 2D bis(diimino)nickel framework acting as the cathode of LIBs with a specific capacity of 155

mAh g^{-1} due to its multi redox states accompanied by both cation and anion insertion/desertion during charge/discharge processes.[219] Although it is still in very early stage, the performance results are comparable to other commercially used materials in LIBs, showing their potential in the nearly unexplored electrochemical application field.

3.3.2. Supercapacitor

With the rapidly growing research efforts in the field of batteries, supercapacitors (SCs) have also drawn general attention for their distinctive characteristics, such as high power density, long cycle life, high cost-effectiveness, and wide operating temperatures. So far, two distinct routes are identified as the energy storage processes of SCs: 1. non-Faradaic processes arising from the adsorption of ions on the electrochemical double layer (double-layer capacitance); 2. Faradaic processes accomplished by reversible redox processes of electrode materials (pseudocapacitance). Thus, high-surface-area and redox-active materials are highly desired for developing SCs. 2D-MOFs/COFs, emerging as a new class of porous materials with exceptional porosities and high-aspect-ratios, are gaining extensive attentions as suitable candidates for SCs.

Sharing the common challenges of stability and conductivity, 2D-COFs are structurally modified to achieve high capacity and long cycling life.[220] On one hand, to increase the pseudocapacitance, the incorporation of redox-active species/groups seems essential for the use of COFs as SCs material, as suggested by the work of Tang *et al*.[221] who reported a 2D-COF material with redox active pyridine units as the SCs electrode. Owing to the easily accessible units on the surface, a specific capacitance of 102 F g^{-1} (at 0.5 A g^{-1}) was achieved and remained stable after 6,000 charge/discharge cycles with 92% of capacitance retention. On the other hand, enlarging the surface area is the most accessible way to increase the double-layer capacitance. In 2015, Dichtel and co-workers constructed an oriented thin film of a redox-active 2D-COF on the

Au surface.[222] Comparing to bulk samples, a large proportion (80~99%) of the anthraquinone groups in the thin 2D-COF composite are electrochemically accessible, resulting in a charge storage capabilities increase from 0.4 to 3 mF cm^{-2}.

The incorporation of redox-active groups is not critical for 2D-MOFs because of the various redox states of evenly distributed native metal nodes that contribute to pseudocapacitance.[223, 224] For example, Huang *et al.* presented a porous 2D Ni-MOF material fabricated as SCs electrode in KOH electrolyte,[225] which showed a specific capacity of 125 F g^{-1} with a current density of 0.5 A g^{-1}. The redox between coordinated Ni(II) and Ni(III) was found to be responsible for the charge storage.

4. Conclusion and outlook

In summary, we have summarized synthetic strategies for 2D-MOFs and 2D-COFs in the first part. Currently, two methods are most widely used, self-assembly and decomposition methods. The commonly used ligands and their resulting morphologies are summarized in the review. With the discovery of new types of 2D-MOFs/COFs and the improvement of synthetic methods, their distinct and flexible properties, such as conductivity, thermal and chemical stability, high-aspect-ratio, and well-defined porous structures, have led to their recent popularity in energy-related applications. From separation to gas storage, 2D-MOFs/COFs have demonstrated their high efficiency comparing to bulk MOFs/COFs and conventional materials. In the field of energy conversions, such as CO_2 reduction, water splitting reaction, and oxygen reduction, the flexible 2D-frameworks can be endued with desired properties, such as high conductivity, specific binding sites, electronic and geometric tuning of active sites, and photochemical properties, *via* metal doping and organic functionalization, *etc*. As to the relatively new area of battery and

supercapacitor, both 2D-frameworks have shown the potentials as electrode materials with comparable performances to the conventional materials.

However, the number of reports on the energy-related applications of 2D-MOFs/COFs are still negligible compared to that on their synthesis. One of the reasons is the difficulty of obtaining high-quality 2D-MOFs/COFs without defects. For example, although many 2D materials, including 2D-MOFs/COFs, have been predicted to have metallic and even superconductive properties for some cases,[226] only few experiments have succeeded in preparing them with desired properties due to the limitation of synthetic methods.[114] The resulting low conductivity of current 2D-MOFs/COFs has been hindering the more general application of them in electrochemical processes, including electrocatalysis and energy storage. Moreover, the structurally defected 2D-MOFs/COFs are more likely to dissociate during electronic and structural evolutions. Another drawback of current 2D-MOFs/COFs applications lies in the lack of critical understanding of reaction mechanisms. Compared to that of conventional materials, only a few reaction routes have been identified or proposed,[183, 218] preventing the rational design of 2D-MOFs/COFs for specific needs. The understanding, selection, and tuning of active sites and organic linkers are still at the primitive stage, as well as the control of their properties using doping, functionalization, and hybridization methods. Thus, more works are needed and expected to grow in both synthesis and mechanism studies, to realize wider applications of 2D-MOFs/COFs in energy-related fields.

Conflict of interest

There are no conflicts of interest to declare.

Acknowledgements

This work was supported by the Innovation and Technology Commission, The Hong Kong Polytechnic University (Grant No. G-YBSZ and 1-BE0Y). KYW acknowledged the support by the Patrick S.C. Poon endowed professorship.

List of abbreviations

References

[1] P. Das, Q. Fu, X. Bao, Z.-S. Wu, Journal of Materials Chemistry A, (2018).

[2] M. Velický, P.S. Toth, Applied Materials Today, 8 (2017) 68-103.

[3] H. Zhang, Chemical Reviews, 118 (2018) 6089-6090.

[4] B. Anasori, M.R. Lukatskaya, Y. Gogotsi, Nature Reviews Materials, 2 (2017) 16098.

[5] V.M. Hong Ng, H. Huang, K. Zhou, P.S. Lee, W. Que, J.Z. Xu, L.B. Kong, Journal of Materials Chemistry A, 5 (2017) 3039-3068.

[6] J. Zhu, E. Ha, G. Zhao, Y. Zhou, D. Huang, G. Yue, L. Hu, N. Sun, Y. Wang, L.Y.S. Lee, C. Xu, K.-Y. Wong, D. Astruc, P. Zhao, Coordination Chemistry Reviews, 352 (2017) 306-327.

[7] A. Naseri, M. Samadi, A. Pourjavadi, A.Z. Moshfegh, S. Ramakrishna, Journal of Materials Chemistry A, 5 (2017) 23406-23433.

[8] J. Zhu, P. Xiao, H. Li, S.A.C. Carabineiro, ACS Applied Materials & Interfaces, 6 (2014) 16449-16465.

[9] S. Meng, Z. Lingxia, S. Jianlin, Nanotechnology, 29 (2018) 412001.

[10] Q. Wang, D. O'Hare, Chemical Reviews, 112 (2012) 4124-4155.

[11] L. Mohapatra, K. Parida, Journal of Materials Chemistry A, 4 (2016) 10744-10766.

[12] K. Yan, G. Wu, W. Jin, Energy Technology, 4 (2016) 354-368.

[13] X. Zheng, J. Luo, W. Lv, D.-W. Wang, Q.-H. Yang, Advanced Materials, 27 (2015) 5388-5395.

[14] M. Hartmann, W. Schwieger, Chemical Society Reviews, 45 (2016) 3311-3312.

[15] M.-H. Sun, S.-Z. Huang, L.-H. Chen, Y. Li, X.-Y. Yang, Z.-Y. Yuan, B.-L. Su, Chemical Society Reviews, 45 (2016) 3479-3563.

[16] M.E. Davis, Nature, 417 (2002) 813.

[17] C.S. Diercks, Y. Liu, K.E. Cordova, O.M. Yaghi, Nature Materials, 17 (2018) 301-307.

[18] H. Wang, Q.-L. Zhu, R. Zou, Q. Xu, Chem, 2 (2017) 52-80.

[19] G. Xu, P. Nie, H. Dou, B. Ding, L. Li, X. Zhang, Materials Today, 20 (2017) 191-209.

[20] Y. Yan, T. He, B. Zhao, K. Qi, H. Liu, B.Y. Xia, Journal of Materials Chemistry A, 6 (2018) 15905-15926.

[21] U. Rychlewska, B. Warzajtis, M.D. Dimitrijevic, N.S. Draskovic, M.I. Djuran, Acta Crystallogr Sect E Struct Rep Online, 65 (2009) m648-649.

[22] O.Q. Munro, M.P. Akerman, K. Gillham, Acta Crystallogr., Sect. C: Cryst. Struct. Commun., 65 (2009) m343-m346.

[23] V.S. Dhanya, M.R. Sudarsanakumar, S. Suma, S.W. Ng, M.S. Augustine, S.M. Roy, Inorg. Chem. Commun., 35 (2013) 140-143.

[24] Y. Peng, Y. Li, Y. Ban, W. Yang, Y. Peng, Angew Chem Int Ed Engl, 56 (2017) 9757-9761.

[25] E.P. Zhang, L.L. Zhang, Z. Tan, Z.G. Ji, Q.W. Li, Chinese J Chem, 34 (2016) 233-238.

[26] D. Yue, Y.K. Huang, J. Zhang, X. Zhang, Y.J. Cui, Y. Yang, G.D. Qian, Eur J Inorg Chem, 2018 (2018) 173-177.

[27] M. Bagherzadeh, F. Ashouri, M. Dakovic, J Solid State Chem, 223 (2015) 32-37.

[28] D. Zhu, C. Guo, J. Liu, L. Wang, Y. Du, S.Z. Qiao, Chem Commun (Camb), 53 (2017) 10906-10909.

[29] L. Ding, J.C. Zhong, X.T. Qiu, Y.Q. Sun, Y.P. Chen, J Solid State Chem, 246 (2017) 138-144.

[30] A. Kondo, H. Noguchi, L. Carlucci, D.M. Proserpio, G. Ciani, H. Kajiro, T. Ohba, H. Kanoh, K. Kaneko, J Am Chem Soc, 129 (2007) 12362-12363.

[31] A.V. Mossine, C.M. Mayhan, D.A. Fowler, S.J. Teat, C.A. Deakyne, J.L. Atwood, Chem. Sci., 5 (2014) 2297-2303.

[32] S. Huh, S. Jung, Y. Kim, S.J. Kim, S. Park, Dalton Trans, 39 (2010) 1261-1265.

[33] J. Xie, Zeitschrift für anorganische und allgemeine Chemie, 635 (2009) 384-388.

[34] M. Zhang, G. Feng, Z. Song, Y.P. Zhou, H.Y. Chao, D. Yuan, T.T. Tan, Z. Guo, Z. Hu, B.Z. Tang, B. Liu, D. Zhao, J Am Chem Soc, 136 (2014) 7241-7244.

[35] C. Livage, N. Guillou, J. Chaigneau, P. Rabu, Mater Res Bull, 41 (2006) 981-986.

[36] Y. Jiang, G.H. Ryu, S.H. Joo, X. Chen, S.H. Lee, X. Chen, M. Huang, X. Wu, D. Luo, Y. Huang, J.H. Lee, B. Wang, X. Zhang, S.K. Kwak, Z. Lee, R.S. Ruoff, ACS Appl Mater Interfaces, 9 (2017) 28107-28116.

[37] C.M. Liu, D.Q. Zhang, X. Hao, D.B. Zhu, Sci Rep, 7 (2017) 11156.

[38] G.S. Papaefstathiou, T. Friscic, L.R. MacGillivray, J Am Chem Soc, 127 (2005) 14160-14161.

[39] S.C. King, H.L. Wang, H.D. Arman, B.L. Chen, Inorg Chem Commun, 74 (2016) 98-101.

[40] D. Sheberla, L. Sun, M.A. Blood-Forsythe, S. Er, C.R. Wade, C.K. Brozek, A. Aspuru-Guzik, M. Dinca, J Am Chem Soc, 136 (2014) 8859-8862.

[41] E.M. Miner, T. Fukushima, D. Sheberla, L. Sun, Y. Surendranath, M. Dinca, Nat Commun, 7 (2016) 10942.

[42] T. Kambe, R. Sakamoto, K. Hoshiko, K. Takada, M. Miyachi, J.H. Ryu, S. Sasaki, J. Kim, K. Nakazato, M. Takata, H. Nishihara, J Am Chem Soc, 135 (2013) 2462-2465.

[43] T. Kambe, R. Sakamoto, T. Kusamoto, T. Pal, N. Fukui, K. Hoshiko, T. Shimojima, Z. Wang, T. Hirahara, K. Ishizaka, S. Hasegawa, F. Liu, H. Nishihara, J Am Chem Soc, 136 (2014) 14357-14360.

[44] A.J. Clough, J.W. Yoo, M.H. Mecklenburg, S.C. Marinescu, J Am Chem Soc, 137 (2015) 118-121.

[45] A. Sengupta, S. Datta, C. Su, T.S. Herng, J. Ding, J.J. Vittal, K.P. Loh, ACS Appl Mater Interfaces, 8 (2016) 16154-16159.

[46] T. He, B. Ni, S. Zhang, Y. Gong, H. Wang, L. Gu, J. Zhuang, W. Hu, X. Wang, Small, 14 (2018) 1703929-1703924.

[47] Y. Huang, M. Zhao, S. Han, Z. Lai, J. Yang, C. Tan, Q. Ma, Q. Lu, J. Chen, X. Zhang, Z. Zhang, B. Li, B. Chen, Y. Zong, H. Zhang, Adv Mater, 29 (2017).

[48] N.C. Smythe, D.P. Butler, C.E. Moore, W.R. McGowan, A.L. Rheingold, L.G. Beauvais, Dalton Trans, 41 (2012) 7855-7858.

[49] H. Nagatomi, N. Yanai, T. Yamada, K. Shiraishi, N. Kimizuka, Chemistry-a European Journal, 24 (2018) 1806-1810.

[50] H. Jia, Y. Yao, J. Zhao, Y. Gao, Z. Luo, P. Du, Journal of Materials Chemistry A, 6 (2018) 1188-1195.

[51] L. Wang, M. Yang, Z. Shi, Y. Chen, S. Feng, J Solid State Chem, 178 (2005) 3359-3365.

[52] R. Dong, Z. Zheng, D.C. Tranca, J. Zhang, N. Chandrasekhar, S. Liu, X. Zhuang, G. Seifert, X. Feng, Chemistry – A European Journal, 23 (2017) 2255-2260.

[53] R. Makiura, S. Motoyama, Y. Umemura, H. Yamanaka, O. Sakata, H. Kitagawa, Nat Mater, 9 (2010) 565-571.

[54] A. Ciesielski, S. Colella, L. Zalewski, B. Bruchmann, P. Samori, Crystengcomm, 13 (2011) 5535-5537.

[55] X.-W. Wang, M.-X. Liu, W.-J. Jiang, T.-J. Cai, Q. Deng, Zeitschrift für Naturforschung B, 64 (2009) 1016-1020.

[56] X. Zhu, J.-W. Zhao, B.-L. Li, Y. Song, Y.-M. Zhang, Y. Zhang, Inorg. Chem., 49 (2010) 1266-1270.

[57] S.A. Bourne, J.J. Lu, A. Mondal, B. Moulton, M.J. Zaworotko, Angew Chem Int Edit, 40 (2001) 2111-2113.

[58] Z. Guo, D.K. Panda, K. Maity, D. Lindsey, T.G. Parker, T.E. Albrecht-Schmitt, J.L. Barreda-Esparza, P. Xiong, W. Zhou, S. Saha, Journal of Materials Chemistry C, 4 (2016) 894-899.

[59] L. Huang, X.P. Zhang, Y.J. Han, Q.Q. Wang, Y.X. Fang, S.J. Dong, Journal of Materials Chemistry A, 5 (2017) 18610-18617.

[60] G.W. Zhan, H.C. Zeng, Adv Funct Mater, 26 (2016) 3268-3281.

[61] F. Cao, M. Zhao, Y. Yu, B. Chen, Y. Huang, J. Yang, X. Cao, Q. Lu, X. Zhang, Z. Zhang, C. Tan, H. Zhang, J Am Chem Soc, 138 (2016) 6924-6927.

[62] L. Ye, Y. Gao, S.Y. Cao, H. Chen, Y. Yao, J.G. Hou, L.C. Sun, Appl Catal B-Environ, 227 (2018) 54-60.

[63] L. He, F. Duan, Y. Song, C. Guo, H. Zhao, J.-Y. Tian, Z. Zhang, C.-S. Liu, X. Zhang, P. Wang, M. Du, S.-M. Fang, 2D Materials, 4 (2017).

[64] S.M. Chen, M. Liu, Z.G. Gu, W.Q. Fu, J. Zhang, ACS Appl Mater Interfaces, 8 (2016) 27332-27338.

[65] T. Deng, W. Zhang, O. Arcelus, D. Wang, X.Y. Shi, X.Y. Zhang, J. Carrasco, T. Rojo, W.T. Zheng, Commun Chem, 1 (2018).

[66] J. Duan, S. Chen, C. Zhao, Nat Commun, 8 (2017) 15341-15348.

[67] C. Kutzscher, A. Gelbert, S. Ehrling, C. Schenk, I. Senkovska, S. Kaskel, Dalton Trans, 46 (2017) 16480-16484.

[68] H.L. Liu, Y.J. Chang, T. Fan, Z.Y. Gu, Chem Commun (Camb), 52 (2016) 12984-12987.

[69] M.J. Cliffe, E. Castillo-Martinez, Y. Wu, J. Lee, A.C. Forse, F.C.N. Firth, P.Z. Moghadam, D. Fairen-Jimenez, M.W. Gaultois, J.A. Hill, O.V. Magdysyuk, B. Slater, A.L. Goodwin, C.P. Grey, J Am Chem Soc, 139 (2017) 5397-5404.

[70] S. Wan, J. Guo, J. Kim, H. Ihee, D. Jiang, Angewandte Chemie International Edition, 47 (2008) 8826-8830.

[71] R.W. Tilford, S.J. Mugavero, P.J. Pellechia, J.J. Lavigne, Advanced Materials, 20 (2008) 2741-2746.

[72] E.L. Spitler, W.R. Dichtel, Nature Chemistry, 2 (2010) 672.

[73] S. Bhunia, S.K. Das, S. Bhattacharya, A. Bhaumik, A. Pradhan, R. Jana, S.C. Peter, M. Addicoat, ACS Appl Mater Interfaces, 9 (2017) 23843-23851.

[74] B.J. Smith, A.C. Overholts, N. Hwang, W.R. Dichtel, Chem Commun (Camb), 52 (2016) 3690-3693.

[75] A.P. Côté, A.I. Benin, N.W. Ockwig, M. O'Keeffe, A.J. Matzger, O.M. Yaghi, Science, 310 (2005) 1166-1170.

[76] L.M. Lanni, R.W. Tilford, M. Bharathy, J.J. Lavigne, Journal of the American Chemical Society, 133 (2011) 13975-13983.

[77] F.J. Uribe-Romo, C.J. Doonan, H. Furukawa, K. Oisaki, O.M. Yaghi, Journal of the American Chemical Society, 133 (2011) 11478-11481.

[78] Q. Fang, Z. Zhuang, S. Gu, R.B. Kaspar, J. Zheng, J. Wang, S. Qiu, Y. Yan, Nature Communications, 5 (2014) 4503.

[79] X. Gou, Q. Zhang, Y. Wu, Y. Zhao, X. Shi, X. Fan, L. Huang, G. Lu, RSC Adv., 6 (2016) 39198-39203.

[80] R.P. Bisbey, C.R. DeBlase, B.J. Smith, W.R. Dichtel, J. Am. Chem. Soc., 138 (2016) 11433-11436.

[81] J.I. Feldblyum, C.H. McCreery, S.C. Andrews, T. Kurosawa, E.J.G. Santos, V. Duong, L. Fang, A.L. Ayzner, Z. Bao, Chem. Commun. (Cambridge, U. K.), 51 (2015) 13894-13897.

[82] Y. Peng, Z. Hu, Y. Gao, D. Yuan, Z. Kang, Y. Qian, N. Yan, D. Zhao, ChemSusChem, 8 (2015) 3208-3212.

[83] Z.-F. Pang, T.-Y. Zhou, R.-R. Liang, Q.-Y. Qi, X. Zhao, Chemical Science, 8 (2017) 3866-3870.

[84] C. Liu, E. Park, Y. Jin, J. Liu, Y. Yu, W. Zhang, S. Lei, W. Hu, Angew. Chem., Int. Ed., 57 (2018) 8984-8988.

[85] R. P P, P.K. Mondal, D. Chopra, Journal of Chemical Sciences, 130 (2018) 51.

[86] J.W. Colson, J.A. Mann, C.R. De Blase, W.R. Dichtel, J. Polym. Sci., Part A: Polym. Chem., 53 (2015) 378-384.

[87] S.-L. Cai, K. Zhang, J.-B. Tan, S. Wang, S.-R. Zheng, J. Fan, Y. Yu, W.-G. Zhang, Y. Liu, ACS Macro Lett., 5 (2016) 1348-1352.

[88] L.A. Baldwin, J.W. Crowe, M.D. Shannon, C.P. Jaroniec, P.L. McGrier, Chemistry of Materials, 27 (2015) 6169-6172.

[89] S.-Q. Xu, R.-R. Liang, T.-G. Zhan, Q.-Y. Qi, X. Zhao, Chemical Communications, 53 (2017) 2431-2434.

[90] T. Sick, A.G. Hufnagel, J. Kampmann, I. Kondofersky, M. Calik, J.M. Rotter, A. Evans, M. Döblinger, S. Herbert, K. Peters, D. Böhm, P. Knochel, D.D. Medina, D. Fattakhova-Rohlfing, T. Bein, Journal of the American Chemical Society, 140 (2018) 2085-2092.

[91] P. Wang, Q. Xu, Z. Li, W. Jiang, Q. Jiang, D. Jiang, Advanced Materials, 30 (2018) 1801991.

[92] S.-Y. Ding, J. Gao, Q. Wang, Y. Zhang, W.-G. Song, C.-Y. Su, W. Wang, Journal of the American Chemical Society, 133 (2011) 19816-19822.

[93] Y. Peng, Y. Huang, Y. Zhu, B. Chen, L. Wang, Z. Lai, Z. Zhang, M. Zhao, C. Tan, N. Yang, F. Shao, Y. Han, H. Zhang, J. Am. Chem. Soc., 139 (2017) 8698-8704.

[94] K. Wang, L.-M. Yang, X. Wang, L. Guo, G. Cheng, C. Zhang, S. Jin, B. Tan, A. Cooper, Angewandte Chemie International Edition, 56 (2017) 14149-14153.

[95] T. Wang, R. Xue, H. Chen, P. Shi, X. Lei, Y. Wei, H. Guo, W. Yang, New Journal of Chemistry, 41 (2017) 14272-14278.

[96] X. Han, J. Zhang, J. Huang, X. Wu, D. Yuan, Y. Liu, Y. Cui, Nature Communications, 9 (2018) 1294.

[97] A.M. Khattak, Z. Ali Ghazi, B. Liang, N. Ali Khan, A. Iqbal, L. Li, Z. Tang, J. Mater. Chem. A, 4 (2016) 16312-16317.

[98] P. Bhanja, K. Bhunia, S.K. Das, D. Pradhan, R. Kimura, Y. Hijikata, S. Irle, A. Bhaumik, ChemSusChem, 10 (2017) 921-929.

[99] S.K. Das, K. Bhunia, A. Mallick, A. Pradhan, D. Pradhan, A. Bhaumik, Microporous and Mesoporous Materials, 266 (2018) 109-116.

[100] S. Wan, J. Guo, J. Kim, H. Ihee, D. Jiang, Angewandte Chemie International Edition, 48 (2009) 5439-5442.

[101] J.W. Colson, A.R. Woll, A. Mukherjee, M.P. Levendorf, E.L. Spitler, V.B. Shields, M.G. Spencer, J. Park, W.R. Dichtel, Science (Washington, DC, U. S.), 332 (2011) 228-231.

[102] E.L. Spitler, B.T. Koo, J.L. Novotney, J.W. Colson, F.J. Uribe-Romo, G.D. Gutierrez, P. Clancy, W.R. Dichtel, J. Am. Chem. Soc., 133 (2011) 19416-19421.

[103] L. Wang, B. Dong, R. Ge, F. Jiang, J. Xu, ACS Appl. Mater. Interfaces, 9 (2017) 7108-7114.

[104] X. Ding, L. Chen, Y. Honsho, X. Feng, O. Saengsawang, J. Guo, A. Saeki, S. Seki, S. Irle, S. Nagase, V. Parasuk, D. Jiang, Journal of the American Chemical Society, 133 (2011) 14510-14513.

[105] X. Ding, J. Guo, X. Feng, Y. Honsho, J. Guo, S. Seki, P. Maitarad, A. Saeki, S. Nagase, D. Jiang, Angewandte Chemie International Edition, 50 (2011) 1289-1293.

[106] V.S.P.K. Neti, X. Wu, S. Deng, L. Echegoyen, CrystEngComm, 15 (2013) 6892-6895.

[107] V.S.P.K. Neti, X. Wu, M. Hosseini, R.A. Bernal, S. Deng, L. Echegoyen, Crystengcomm, 15 (2013) 7157-7160.

[108] X. Feng, L. Chen, Y. Dong, D. Jiang, Chemical Communications, 47 (2011) 1979-1981.

[109] A. Nagai, X. Chen, X. Feng, X. Ding, Z. Guo, D. Jiang, Angewandte Chemie International Edition, 52 (2013) 3770-3774.

[110] H. Yang, S. Zhang, L. Han, Z. Zhang, Z. Xue, J. Gao, Y. Li, C. Huang, Y. Yi, H. Liu, Y. Li, ACS Appl. Mater. Interfaces, 8 (2016) 5366-5375.

[111] C. Zhang, S. Zhang, Y. Yan, F. Xia, A. Huang, Y. Xian, ACS Applied Materials & Interfaces, 9 (2017) 13415-13421.

[112] C.S. Diercks, N. Kornienko, E.A. Kapustin, E.M. Nichols, C. Zhu, Y. Zhao, C.J. Chang, O.M. Yaghi, S. Lin, J Am Chem Soc, 140 (2018) 1116-1122.

[113] X. Ding, L. Chen, Y. Honsho, X. Feng, O. Saengsawang, J. Guo, A. Saeki, S. Seki, S. Irle, S. Nagase, V. Parasuk, D. Jiang, J Am Chem Soc, 133 (2011) 14510-14513.

[114] A.J. Clough, J.M. Skelton, C.A. Downes, A.A. de la Rosa, J.W. Yoo, A. Walsh, B.C. Melot, S.C. Marinescu, J Am Chem Soc, 139 (2017) 10863-10867.

[115] M. Zhao, Y. Huang, Y. Peng, Z. Huang, Q. Ma, H. Zhang, Chem Soc Rev, 47 (2018) 6267-6295.

[116] M. Zhao, Q. Lu, Q. Ma, H. Zhang, Small Methods, 1 (2017) 1600030-1600038.

[117] J. Cong, H. Xu, M. Lu, Y. Wu, Y. Li, P. He, J. Gao, J. Yao, S. Xu, Chem-Asian J, 13 (2018) 1485-1491.

[118] Z.X. Kang, L.L. Fan, D.F. Sun, Journal of Materials Chemistry A, 5 (2017) 10073-10091.

[119] D. Zhao, D.J. Timmons, D. Yuan, H.C. Zhou, Accounts Chem Res, 44 (2011) 123-133.

[120] X. Zhu, C.C. Tian, C.L. Do-Thanh, S. Dai, Chemsuschem, 10 (2017) 3304-3316.

[121] M. Tong, Q. Yang, Q. Ma, D. Liu, C. Zhong, Journal of Materials Chemistry A, 4 (2016) 124-131.

[122] X.J. Hong, Q. Wei, Y.P. Cai, B.B. Wu, H.X. Feng, Y. Yu, R.F. Dong, ACS Appl Mater Interfaces, 9 (2017) 29374-29379.

[123] L.H. Wee, M. Meledina, S. Turner, G. Van Tendeloo, K. Zhang, L.M. Rodriguez-Albelo, A. Masala, S. Bordiga, J. Jiang, J.A. Navarro, C.E. Kirschhock, J.A. Martens, J Am Chem Soc, 139 (2017) 819-828.

[124] J.R. Li, R.J. Kuppler, H.C. Zhou, Chem Soc Rev, 38 (2009) 1477-1504.

[125] J.L. Segura, M.J. Mancheno, F. Zamora, Chem Soc Rev, 45 (2016) 5635-5671.

[126] B.P. Biswal, H.D. Chaudhari, R. Banerjee, U.K. Kharul, Chemistry-a European Journal, 22 (2016) 4695-4699.

[127] J. Fu, S. Das, G. Xing, T. Ben, V. Valtchev, S. Qiu, J Am Chem Soc, 138 (2016) 7673-7680.

[128] Y.P. Ying, D.H. Liu, J. Ma, M.M. Tong, W.X. Zhang, H.L. Huang, Q.Y. Yang, C.L. Zhong, Journal of Materials Chemistry A, 4 (2016) 13444-13449.

[129] H. Fan, A. Mundstock, A. Feldhoff, A. Knebel, J. Gu, H. Meng, J. Caro, J Am Chem Soc, 140 (2018) 10094-10098.

[130] G. Li, K. Zhang, T. Tsuru, ACS Appl Mater Interfaces, 9 (2017) 8433-8436.

[131] Y. Peng, Y. Li, Y. Ban, H. Jin, W. Jiao, X. Liu, W. Yang, Science, 346 (2014) 1356-1359.

[132] Y. Peng, Y. Li, Y. Ban, W. Yang, Angew Chem Int Ed Engl, 56 (2017) 9757-9761.

[133] Y.D. He, J. Shang, Q.F. Gu, G. Li, J.Y. Li, R. Singh, P. Xiao, P.A. Webley, Chem Commun, 51 (2015) 14716-14719.

[134] W.B. Li, Y.F. Zhang, P.C. Su, Z.H. Xu, G.L. Zhang, C. Shen, Q. Meng, Journal of Materials Chemistry A, 4 (2016) 18747-18752.

[135] Y. Li, H. Liu, H. Wang, J. Qiu, X. Zhang, Chem Sci, 9 (2018) 4132-4141.

[136] Y.J. Li, L. Lin, M. Tu, P. Nian, A.J. Howarth, O.K. Farha, J.S. Qiu, X.F. Zhang, Nano Res, 11 (2018) 1850-1860.

[137] T. Rodenas, I. Luz, G. Prieto, B. Seoane, H. Miro, A. Corma, F. Kapteijn, I.X.F.X. Llabres, J. Gascon, Nature Materials, 14 (2015) 48-55.

[138] Y.D. Cheng, X.R. Wang, C.K. Jia, Y.X. Wang, L.Z. Zhai, Q. Wang, D. Zhao, J Membrane Sci, 539 (2017) 213-223.

[139] M.H. Zhang, Z.Q. Qi, Y. Feng, B.B. Guo, Y.J. Hao, Z. Xu, L.L. Zhang, D.F. Sun, Inorg Chem Front, 5 (2018) 1314-1320.

[140] A.M. Nasir, N.A.H.M. Nordin, P.S. Goh, A.F. Ismail, J Mol Liq, 250 (2018) 269-277.

[141] H. Ang, L. Hong, ACS Appl Mater Interfaces, 9 (2017) 28079-28088.
[142] D. Cui, J.M. MacLeod, M. Ebrahimi, F. Rosei, Crystengcomm, 19 (2017) 4927-4932.
[143] J. Sun, X. Zhou, S. Lei, Chem Commun (Camb), 52 (2016) 8691-8694.
[144] Z.F. Pang, T.Y. Zhou, R.R. Liang, Q.Y. Qi, X. Zhao, Chem Sci, 8 (2017) 3866-3870.
[145] P. Wang, Q. Xu, Z. Li, W. Jiang, Q. Jiang, D. Jiang, Adv Mater, 30 (2018) 1801991-1801997.
[146] C. Liu, E. Park, Y. Jin, J. Liu, Y. Yu, W. Zhang, S. Lei, W. Hu, Angewandte Chemie International Edition, 57 (2018) 8984-8988.
[147] D. Cui, J.M. MacLeod, M. Ebrahimi, D.F. Perepichka, F. Rosei, Chem Commun (Camb), 51 (2015) 16510-16513.
[148] S.Y. Ding, W. Wang, Chem Soc Rev, 42 (2013) 548-568.
[149] H.B. Zhang, J.W. Nai, L. Yu, X.W. Lou, Joule, 1 (2017) 77-107.
[150] R. Babarao, J.W. Jiang, Energ Environ Sci, 1 (2008) 139-143.
[151] J. Yu, L.H. Xie, J.R. Li, Y. Ma, J.M. Seminario, P.B. Balbuena, Chem Rev, 117 (2017) 9674-9754.
[152] V.A. Blagojevic, V. Lukic, N.N. Begavic, A.M. Maricic, D.M. Minic, International Journal of Hydrogen Energy, 41 (2016) 22171-22181.
[153] Z. Ozturk, D.A. Kose, Z.S. Sahin, G. Ozkan, A. Asan, International Journal of Hydrogen Energy, 41 (2016) 12167-12174.
[154] A. Kondo, H. Noguchi, S. Ohnishi, H. Kajiro, A. Tohdoh, Y. Hattori, W.C. Xu, H. Tanaka, H. Kanoh, K. Kaneko, Nano Lett, 6 (2006) 2581-2584.
[155] I.H. Hwang, J.M. Bae, Y.K. Hwang, H.Y. Kim, C. Kim, S. Huh, S.J. Kim, Y. Kim, Dalton Trans, 42 (2013) 15645-15649.
[156] G.D. Xu, Y.W. Peng, Z.G. Hu, D.Q. Yuan, B. Donnadieu, D. Zhao, H.S. Cheng, Rsc Adv, 5 (2015) 47384-47389.
[157] A. Chakraborty, S. Roy, M. Eswaramoorthy, T.K. Maji, Journal of Materials Chemistry A, 5 (2017) 8423-8430.
[158] H.C. Kim, S. Huh, D.N. Lee, Y. Kim, Dalton Trans, 47 (2018) 4820-4826.
[159] P. Chandrasekhar, A. Mukhopadhyay, G. Savitha, J.N. Moorthy, Journal of Materials Chemistry A, 5 (2017) 5402-5412.
[160] J. Zha, X.Y. Zhang, Cryst Growth Des, 18 (2018) 3209-3214.
[161] T. Suzuki, R. Kotani, A. Kondo, K. Maeda, J Phys Chem C, 120 (2016) 21571-21579.

[162] Z. Kang, Y. Peng, Z. Hu, Y. Qian, C. Chi, L.Y. Yeo, L. Tee, D. Zhao, Journal of Materials Chemistry A, 3 (2015) 20801-20810.

[163] R. Kumar, K. Jayaramulu, T.K. Maji, C.N. Rao, Dalton Trans, 43 (2014) 7383-7386.

[164] Y.J. Choi, J.H. Choi, K.M. Choi, J.K. Kang, J Mater Chem, 21 (2011) 1073-1078.

[165] V.S.P.K. Neti, X.F. Wu, S.G. Deng, L. Echegoyen, Crystengcomm, 15 (2013) 6892-6895.

[166] S.L. Cai, K. Zhang, J.B. Tan, S. Wang, S.R. Zheng, J. Fan, Y. Yu, W.G. Zhang, Y. Liu, Acs Macro Lett, 5 (2016) 1348-1352.

[167] S.Q. Xu, R.R. Liang, T.G. Zhan, Q.Y. Qi, X. Zhao, Chem Commun (Camb), 53 (2017) 2431-2434.

[168] S. Kandambeth, A. Mallick, B. Lukose, M.V. Mane, T. Heine, R. Banerjee, J Am Chem Soc, 134 (2012) 19524-19527.

[169] Z. Li, X. Feng, Y. Zou, Y. Zhang, H. Xia, X. Liu, Y. Mu, Chem Commun (Camb), 50 (2014) 13825-13828.

[170] Y. Peng, Z. Hu, Y. Gao, D. Yuan, Z. Kang, Y. Qian, N. Yan, D. Zhao, ChemSusChem, 8 (2015) 3208-3212.

[171] P. Li, S. Regati, R.J. Butcher, H.D. Arman, Z.X. Chen, S.C. Xiang, B.L. Chen, C.G. Zhao, Tetrahedron Lett, 52 (2011) 6220-6222.

[172] Y.J. Ding, Y.P. Chen, X.L. Zhang, L. Chen, Z.H. Dong, H.L. Jiang, H.X. Xu, H.C. Zhou, Journal of the American Chemical Society, 139 (2017) 9136-9139.

[173] L. Hu, G.X. Hao, H.D. Luo, C.X. Ke, G. Shi, J. Lin, X.M. Lin, U.Y. Qazi, Y.P. Cai, Cryst Growth Des, 18 (2018) 2883-2889.

[174] R. Yan, Y. Zhao, H. Yang, X.J. Kang, C. Wang, L.L. Wen, Z.D. Lu, Adv Funct Mater, 28 (2018) 1802021-1802028.

[175] J. Qiao, Y. Liu, F. Hong, J. Zhang, Chem Soc Rev, 43 (2014) 631-675.

[176] W. Zheng, S. Nayak, W. Yuan, Z. Zeng, X. Hong, K.A. Vincent, S.C. Tsang, Chem Commun (Camb), 52 (2016) 13901-13904.

[177] P.-Q. Liao, J.-Q. Shen, J.-P. Zhang, Coordination Chemistry Reviews, 373 (2018) 22-48.

[178] S. Lin, C.S. Diercks, Y.B. Zhang, N. Kornienko, E.M. Nichols, Y. Zhao, A.R. Paris, D. Kim, P. Yang, O.M. Yaghi, C.J. Chang, Science, 349 (2015) 1208-1213.

[179] N. Kornienko, Y. Zhao, C.S. Kley, C. Zhu, D. Kim, S. Lin, C.J. Chang, O.M. Yaghi, P. Yang, Journal of the American Chemical Society, 137 (2015) 14129-14135.

[180] C.A. Trickett, A. Helal, B.A. Al-Maythalony, Z.H. Yamani, K.E. Cordova, O.M. Yaghi, Nature Reviews Materials, 2 (2017) 17045-17060.

[181] R. Li, S.H. Wang, X.X. Chen, J. Lu, Z.H. Fu, Y. Li, G. Xu, F.K. Zheng, G.C. Guo, Chem Mater, 29 (2017) 2321-2331.

[182] Z. Sun, S. Yu, L. Zhao, J. Wang, Z. Li, G. Li, Chem-Eur J, 24 (2018) 10829-10839.

[183] C.S. Diercks, S. Lin, N. Kornienko, E.A. Kapustin, E.M. Nichols, C. Zhu, Y. Zhao, C.J. Chang, O.M. Yaghi, J Am Chem Soc, 140 (2018) 1116-1122.

[184] H. Liu, J. Chu, Z. Yin, X. Cai, L. Zhuang, H. Deng, Chem, 4 (2018) 1696-1709.

[185] P. Patel, B. Parmar, R.I. Kureshy, N.U. Khan, E. Suresh, Chemcatchem, 10 (2018) 2401-2408.

[186] B. Zhu, R. Zou, Q. Xu, Advanced Energy Materials, 8 (2018) 1801193-1801225.

[187] W. Zhang, K. Zhou, Small, 13 (2017) 1700806.

[188] C.A. Downes, A.J. Clough, K. Chen, J.W. Yoo, S.C. Marinescu, ACS Appl Mater Interfaces, 10 (2018) 1719-1727.

[189] R. Dong, M. Pfeffermann, H. Liang, Z. Zheng, X. Zhu, J. Zhang, X. Feng, Angew Chem Int Ed Engl, 54 (2015) 12058-12063.

[190] S. Bhunia, S.K. Das, R. Jana, S.C. Peter, S. Bhattacharya, M. Addicoat, A. Bhaumik, A. Pradhan, ACS Appl Mater Interfaces, 9 (2017) 23843-23851.

[191] J.I. Feldblyum, C.H. McCreery, S.C. Andrews, T. Kurosawa, E.J. Santos, V. Duong, L. Fang, A.L. Ayzner, Z. Bao, Chem Commun (Camb), 51 (2015) 13894-13897.

[192] X. Li, Q. Gao, J. Wang, Y. Chen, Z.H. Chen, H.S. Xu, W. Tang, K. Leng, G.H. Ning, J. Wu, Q.H. Xu, S.Y. Quek, Y. Lu, K.P. Loh, Nat Commun, 9 (2018) 2235-2243.

[193] V. Rubio-Gimenez, M. Galbiati, J. Castells-Gil, N. Almora-Barrios, J. Navarro-Sanchez, G. Escorcia-Ariza, M. Mattera, T. Arnold, J. Rawle, S. Tatay, E. Coronado, C. Marti-Gastaldo, Adv Mater, 30 (2018) 1704291-1704298.

[194] X.R. Wu, X. Shen, S.R. Fan, M. Trivedi, B.H. Li, A. Kumar, J.Q. Liu, Rsc Adv, 8 (2018) 23529-23538.

[195] T. Banerjee, F. Haase, G. Savasci, K. Gottschling, C. Ochsenfeld, B.V. Lotsch, Journal of the American Chemical Society, 139 (2017) 16228-16234.

[196] D.M. Chen, C.X. Sun, C.S. Liu, M. Du, Inorg Chem, 57 (2018) 7975-7981.

[197] V.S. Vyas, F. Haase, L. Stegbauer, G. Savasci, F. Podjaski, C. Ochsenfeld, B.V. Lotsch, Nat Commun, 6 (2015) 8508-8516.

[198] T. Sick, A.G. Hufnagel, J. Kampmann, I. Kondofersky, M. Calik, J.M. Rotter, A. Evans, M. Doblinger, S. Herbert, K. Peters, D. Bohm, P. Knochel, D.D. Medina, D. Fattakhova-Rohlfing, T. Bein, J Am Chem Soc, 140 (2018) 2085-2092.

[199] S.M.J. Rogge, A. Bavykina, J. Hajek, H. Garcia, A.I. Olivos-Suarez, A. Sepulveda-Escribano, A. Vimont, G. Clet, P. Bazin, F. Kapteijn, M. Daturi, E.V. Ramos-Fernandez, I.X.F.X. Llabres, V. Van Speybroeck, J. Gascon, Chem Soc Rev, 46 (2017) 3134-3184.

[200] T. Zhang, J. Du, H. Zhang, C. Xu, Electrochimica Acta, 219 (2016) 623-629.

[201] H.X. Jia, Y.C. Yao, J.T. Zhao, Y.Y. Gao, Z.L. Luo, P.W. Du, Journal of Materials Chemistry A, 6 (2018) 1188-1195.

[202] J. Huang, Y. Li, R.K. Huang, C.T. He, L. Gong, Q. Hu, L. Wang, Y.T. Xu, X.Y. Tian, S.Y. Liu, Z.M. Ye, F. Wang, D.D. Zhou, W.X. Zhang, J.P. Zhang, Angew Chem Int Ed Engl, 57 (2018) 4632-4636.

[203] S.L. Zhao, Y. Wang, J.C. Dong, C.T. He, H.J. Yin, P.F. An, K. Zhao, X.F. Zhang, C. Gao, L.J. Zhang, J.W. Lv, J.X. Wang, J.Q. Zhang, A.M. Khattak, N.A. Khan, Z.X. Wei, J. Zhang, S.Q. Liu, H.J. Zhao, Z.Y. Tang, Nat Energy, 1 (2016) 1-10.

[204] K. Rui, G.Q. Zhao, Y.P. Chen, Y. Lin, Q. Zhou, J.Y. Chen, J.X. Zhu, W.P. Sun, W. Huang, S.X. Dou, Adv Funct Mater, 28 (2018) 1801554-1801552.

[205] M. Liu, W. Zheng, S. Ran, S.T. Boles, L.Y.S. Lee, Advanced Materials Interfaces, (2018) 1800849-1800856.

[206] L. Zhao, B. Dong, S. Li, L. Zhou, L. Lai, Z. Wang, S. Zhao, M. Han, K. Gao, M. Lu, X. Xie, B. Chen, Z. Liu, X. Wang, H. Zhang, H. Li, J. Liu, H. Zhang, X. Huang, W. Huang, ACS Nano, 11 (2017) 5800-5807.

[207] S. Gonen, L. Elbaz, Current Opinion in Electrochemistry, 9 (2018) 179-188.

[208] Z. Xiang, Y. Xue, D. Cao, L. Huang, J.F. Chen, L. Dai, Angew Chem Int Ed Engl, 53 (2014) 2433-2437.

[209] P. Zhang, X. Hou, L. Liu, J. Mi, M. Dong, J Phys Chem C, 119 (2015) 28028-28037.

[210] Y. Tian, Z. Zhang, C. Wu, L. Yan, W. Chen, Z. Su, Phys Chem Chem Phys, 20 (2018) 1821-1828.

[211] E.M. Miner, S. Gul, N.D. Ricke, E. Pastor, J. Yano, V.K. Yachandra, T. Van Voorhis, M. Dinca, Acs Catal, 7 (2017) 7726-7731.

[212] Y. Jiang, H. Liu, X. Tan, L. Guo, J. Zhang, S. Liu, Y. Guo, J. Zhang, H. Wang, W. Chu, ACS Appl Mater Interfaces, 9 (2017) 25239-25249.

[213] K.M. Zhao, S.Q. Liu, G.Y. Ye, Q.M. Gan, Z. Zhou, Z. He, Journal of Materials Chemistry A, 6 (2018) 2166-2175.

[214] C.S. Diercks, O.M. Yaghi, Science, 355 (2017) 1585-1593.

[215] H. Yang, S. Zhang, L. Han, Z. Zhang, Z. Xue, J. Gao, Y. Li, C. Huang, Y. Yi, H. Liu, Y. Li, ACS Appl Mater Interfaces, 8 (2016) 5366-5375.

[216] Z. Lei, Q. Yang, Y. Xu, S. Guo, W. Sun, H. Liu, L.P. Lv, Y. Zhang, Y. Wang, Nat Commun, 9 (2018) 576-588.

[217] B. Tian, G.H. Ning, Q. Gao, L.M. Tan, W. Tang, Z. Chen, C. Su, K.P. Loh, ACS Appl Mater Interfaces, 8 (2016) 31067-31075.

[218] J. Park, M. Lee, D. Feng, Z. Huang, A.C. Hinckley, A. Yakovenko, X. Zou, Y. Cui, Z. Bao, J Am Chem Soc, 140 (2018) 10315-10323.

[219] K. Wada, K. Sakaushi, S. Sasaki, H. Nishihara, Angew Chem Int Ed Engl, 57 (2018) 8886-8890.

[220] M.A. Khayum, V. Vijayakumar, S. Karak, S. Kandambeth, M. Bhadra, K. Suresh, N. Acharambath, S. Kurungot, R. Banerjee, ACS Appl Mater Interfaces, 10 (2018) 28139-28146.

[221] A.M. Khattak, Z.A. Ghazi, B. Liang, N.A. Khan, A. Iqbal, L.S. Li, Z.Y. Tang, Journal of Materials Chemistry A, 4 (2016) 16312-16317.

[222] C.R. DeBlase, K. Hernandez-Burgos, K.E. Silberstein, G.G. Rodriguez-Calero, R.P. Bisbey, H.D. Abruna, W.R. Dichtel, ACS Nano, 9 (2015) 3178-3183.

[223] H.C. Xia, J.N. Zhang, Z. Yang, S.Y. Guo, S.H. Guo, Q. Xu, Nano-Micro Lett, 9 (2017) 43-53.

[224] C.R. Zhang, Q. Zhang, K. Zhang, Z.Y. Xiao, Y. Yang, L. Wang, Rsc Adv, 8 (2018) 17747-17753.

[225] C. Feng, C.P. Lv, Z.Q. Li, H. Zhao, H.H. Huang, J Solid State Chem, 265 (2018) 244-247.

[226] X. Zhang, Y. Zhou, B. Cui, M. Zhao, F. Liu, Nano Lett, 17 (2017) 6166-6170.

Figures (Currently only corresponding to application part)

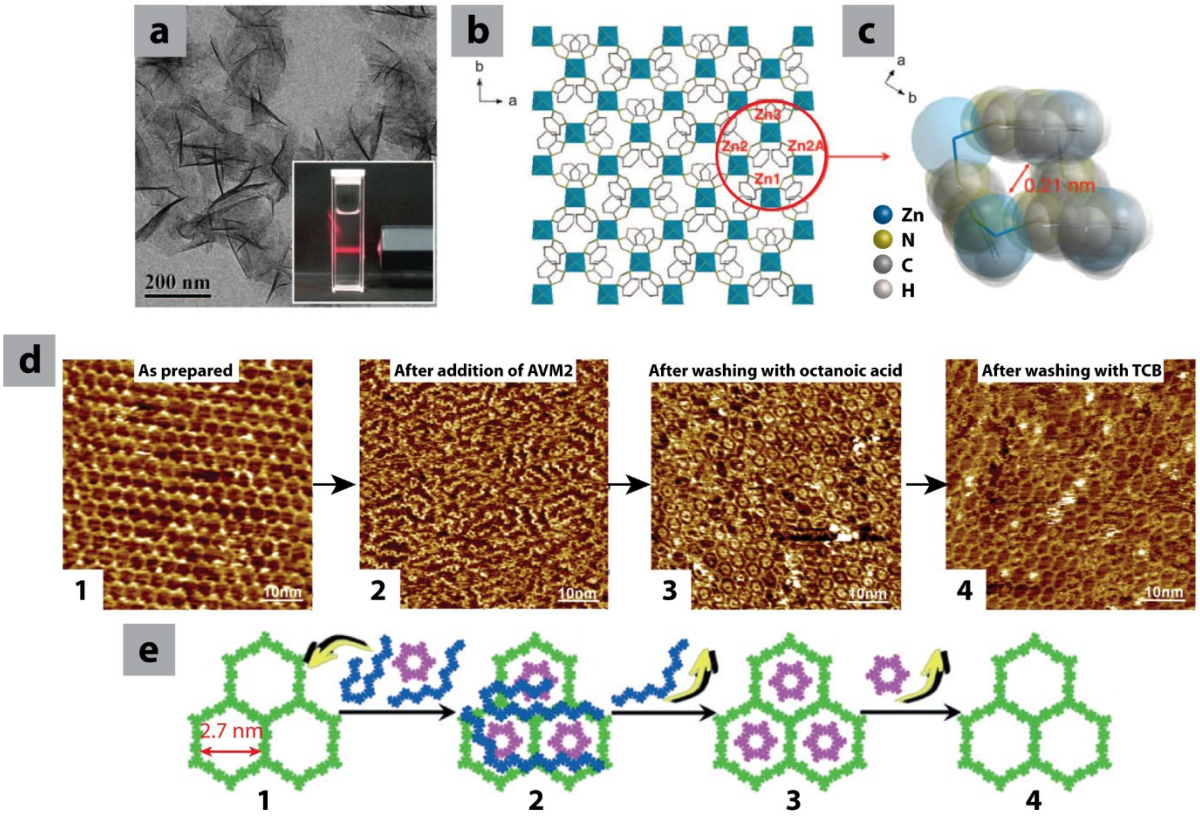

Figure 1. (a) Transmission electron microscopy (TEM) image of $Zn_2(bim)_4$ molecular sieve nanosheets. Inset: the Tyndall effect of a colloidal suspension. (b) Illustration of the grid-like structure of the $Zn_2(bim)_4$ nanosheet. The Zn coordination polyhedra are depicted in blue, whereas the bim links are represented by sticks. (c) Space-filling representation of a four-membered ring of the $Zn_2(bim)_4$ nanosheet. (a-c) Reproduced with permission.[131] Copyright 2014, American Association for the Advancement of Science. (d) Scanning tunnelling microscope (STM) images for the controlled separation of AVM2 from linear by-products using COF. (e) Schematic illustration of the corresponding separation processes. (d-e) Reproduced with permission.[146] Copyright 2018, Wiley-VCH.

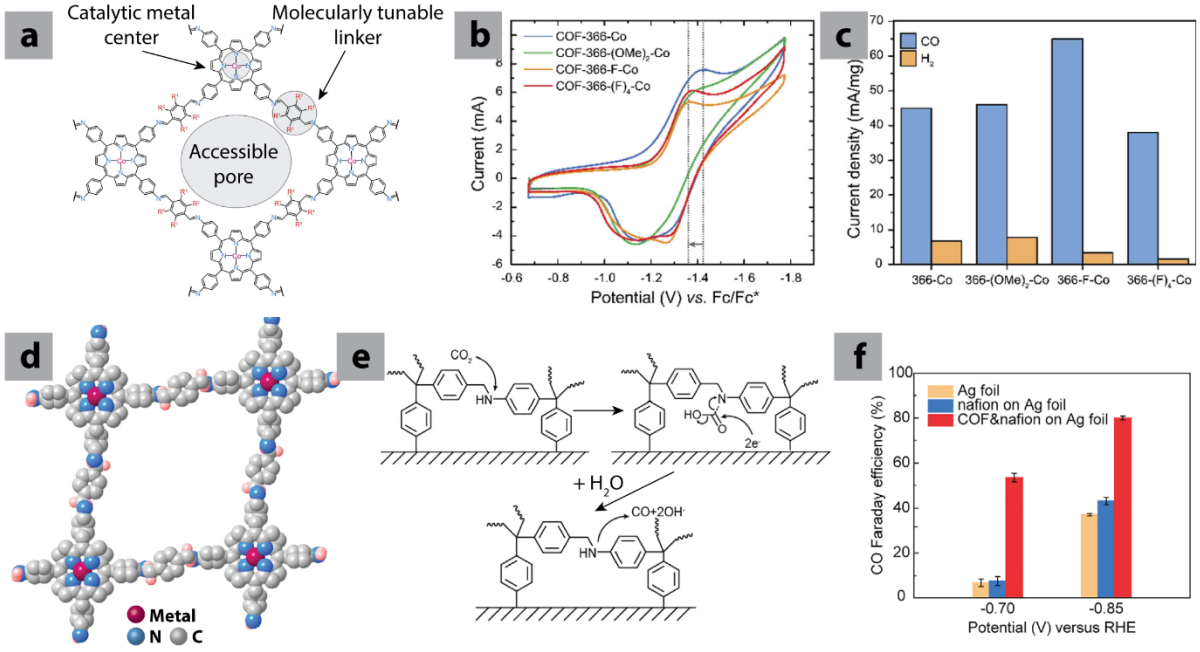

Figure 2. (a) Structure of cobalt-porphyrin COF. (b) Cyclic voltammograms of functionalized Co-COFs (COF-366-Co, COF-366-$(OMe)_2$-Co, COF-366-F-Co, and COF-366-$(F)_4$-Co) in N,N-dimethylformamide with tetrabutylammonium hexafluorophosphate as the electrolyte. (c) Current densities per milligram of cobalt using different COF catalysts (E= −0.67 V *vs.* RHE) in 0.5 M aqueous potassium bicarbonate buffer. (a-c) Reproduced with permission.[183] Copyright 2018, American Chemical Society. (d) Space-filling diagrams of COF-366-M (M=metal) after reduction, metal, carbon and nitrogen atoms are represented as purple, gray and blue spheres, respectively. (e) Scheme of the mechanism of concerted CO_2 reduction at the interface between COFs and the silver electrode *via* the critical carbamate formation. (f) Faradic efficiency for CO using Ag foil, nafion on Ag foil, and COF with nafion on Ag foil. (d-f) Reproduced with permission.[184] Copyright 2018, Elsevier Inc.

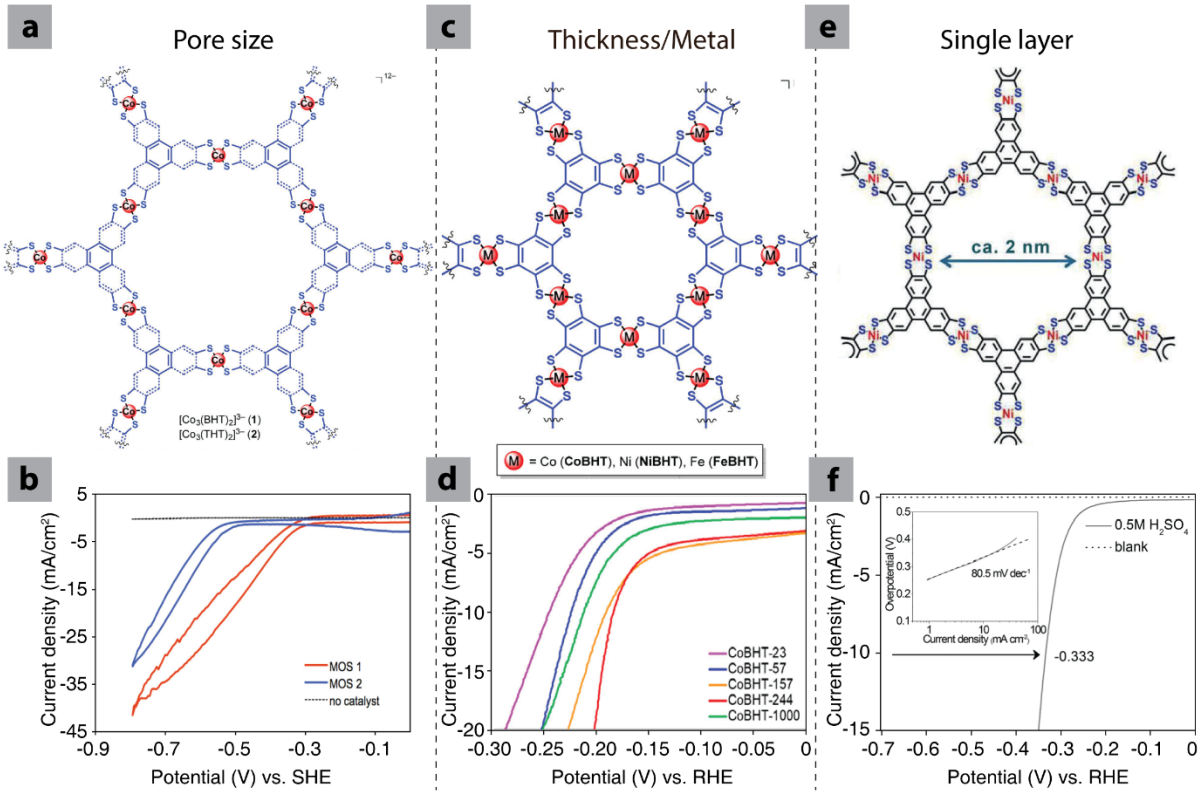

Figure 3. (a) Structure of Cobalt dithiolene MOF, two ligands are used: benzenehexathiol (BHT) and triphenylene-2,3,6,7,10,11-hexathiol (THT). (b) Polarization curves of MOS-1 (Co-BHT MOF) and MOS-2 (Co-THT MOF) in H_2SO_4 solution (pH=1.3). (a-b) Reproduced with permission.[44] Copyright 2015, American Chemical Society. (c) Structure of the MOF with BHT linker. (d) Polarization curves of Co-MOF with different thickness. (c-d) Reproduced with permission.[188] Copyright 2018, American Chemical Society. (e) Structure of Ni-MOF with THT as ligand. (f) Polarization plots of the Ni-MOF sheet in 0.5M H_2SO_4 solution. Inset: the corresponding Tafel plot. (e-f) Reproduced with permission.[189] Copyright 2015, Wiley-VCH.

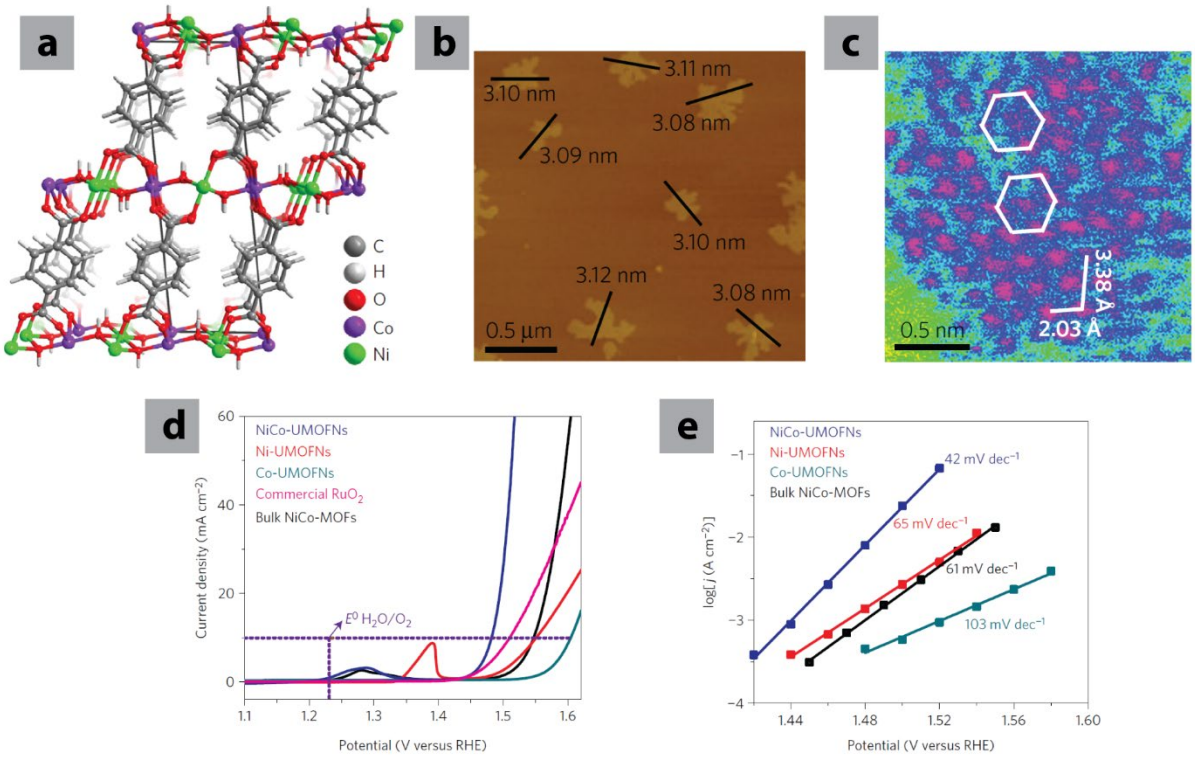

Figure 4. (a) Crystal structure of the ultrathin NiCo-MOF. (b) Atomic force microscopy (AFM) image of as-prepared NiCo-MOF, the thickness values are shown in the image. (c) High-angle annular dark-field scanning transmission electron microscopy (HAADF-STEM) image of the NiCo-MOF showing the hexagonal arrangement of the metal atoms. The metal atoms are shown in pink, carbon and oxygen are shown in blue. (d) OER polarization curves of various MOFs with NiCo, Ni, and Co respectively (NiCo-MOF shown as NiCo-UMOFNs) in O_2-saturated 1M KOH solution at a scan rate of $5mVs^{-1}$. Bulk MOFs and commercial catalyst are shown for comparison. (e) Tafel plots derived from Koutecky–Levich plots of corresponding electrocatalysts. (a-e) Reproduced with permission.[203] Copyright 2016, Nature Publishing Group.

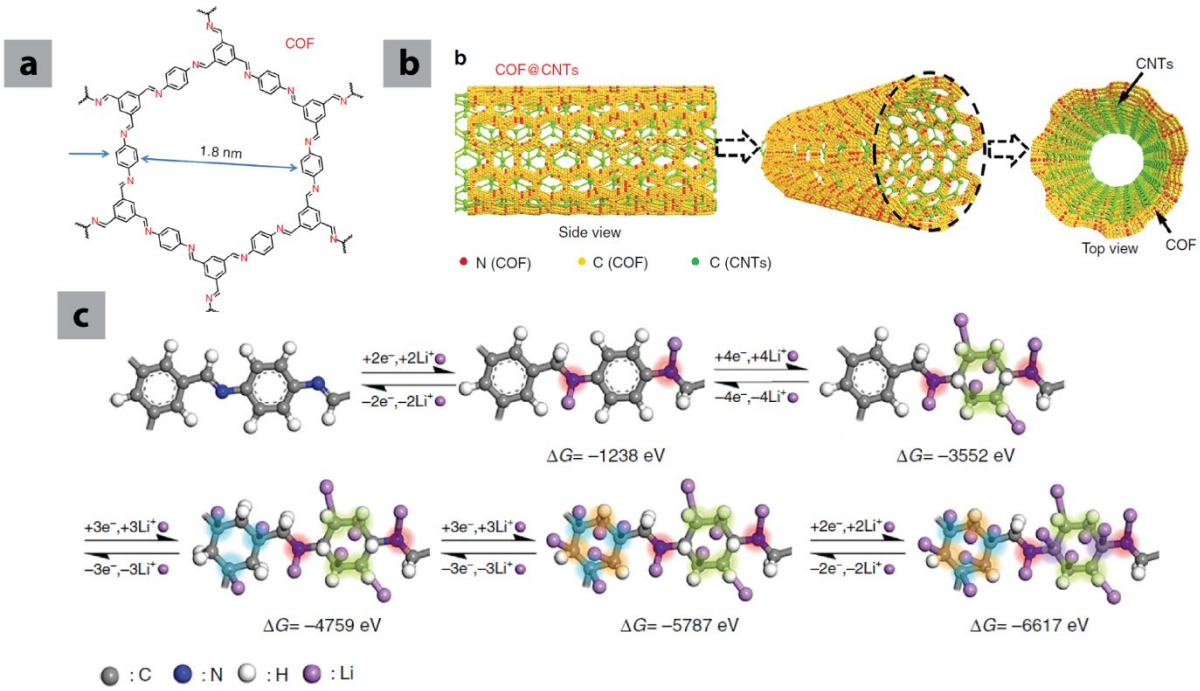

Figure 5. (a) Structure of the 2D-COF. (b) Graphical representation of COF@CNTs with few COF layers covered on the exterior surface of CNTs. (c) Structure evolution of COF units during the lithiation process. The binding sites between lithium and COF are highlighted with red, yellow, blue, orange, and purple colours, respectively. The Gibbs free energy changes are labelled under the corresponding configuration. (a-c) Reproduced with permission.[216] Copyright 2018, Nature Publishing Group.